### ARTICLE IN PRESS

Materials Today: Proceedings xxx (xxxx) xxx



Contents lists available at ScienceDirect

## Materials Today: Proceedings

journal homepage: www.elsevier.com/locate/matpr



# A review on process parameters, microstructure and mechanical properties of additively manufactured AlSi10Mg alloy

Ravindra E. Gite\*, Vishnu D. Wakchaure 1

Department of Mechanical Engineering. Amrutvahini College of Engineering, Sangamner, 422608, (M.S), India

#### ARTICLE INFO

Article history:
Available online xxxx

Keywords:
Additive Manufacturing
Selective Laser Melting
Process Parameters
AlSi10Mg Alloy
Microstructure Mechanical Properties

#### ABSTRACT

Additive Manufacturing is a layer over layer material depositing process to fabricate 3D shape objects. In this process laser completely melts one powder layer and fuses it with another. Metal additive manufacturing process like selective laser melting can produce intricate shapes which are not possible to produce by conventional methods. This capability has enabled designers to come up with innovative part designs which add value to either overall manufacturing process or product performance, also fulfilling the demands for reducing the cost and manufacturing time. The material selection, process parameters and post process are the significant stages in additive manufacturing to achieve the desired properties of output product. The present paper provides comprehensive review in a systematic manner on selective laser melting printing parameters, microstructure, heat treatment and mechanical properties of additively manufactured AlSi10Mg aluminium alloy and based on the review; few arenas for future research are highlighted.

© 2023 Elsevier Ltd. All rights reserved.

Selection and peer-review under responsibility of the scientific committee of the 2nd International Conference and Exposition on Advances in Mechanical Engineering.

#### 1. Introduction

Additive manufacturing (AM) is rapidly growing technology in the era of industry 4.0 and electric vehicles, where the requirements from the industries are changing day by day especially from automotive industries and more focused on strict standards concerning fuel efficiency, air pollution, recycling, and safety. The additive manufacturing technology plays a vital role in the fulfilment of these stringent standards by successfully manufacturing of lightweight structures with complex geometries [1]. This technology provides an infinite design freedom to design engineers for complex geometries that are difficult to produce by conventional methods [2]. The additive manufacturing industry originated 40 years ago, it has transformed significantly from its early days, when the primary market was rapid prototyping. Today this industry is changing at a rapid pace. In metal additive manufacturing technology, Selective Laser Melting (SLM) [3] is one of the favoured technique to produce complex geometries, customized structures, high resolution and accuracy without almost any loss of material

https://doi.org/10.1016/j.matpr.2022.09.100

 $2214\text{-}7853/\text{\circledcirc}\ 2023$  Elsevier Ltd. All rights reserved.

Selection and peer-review under responsibility of the scientific committee of the 2nd International Conference and Exposition on Advances in Mechanical Engineering.

Please cite this article as: R.E. Gite and V.D. Wakchaure, A review on process parameters, microstructure and mechanical properties of additively manufactured AlSi10Mg alloy, Materials Today: Proceedings, https://doi.org/10.1016/j.matpr.2022.09.100

as compare to the traditional technologies [4]. A wide range of materials such as aluminium (Al) and its alloy [5], Inconel (In), Stainless Steel (SS), Titanium (Ti) [6] are commonly used in metal additive manufacturing. In Al-based alloys, AlSi10Mg alloy is highly preferred for various applications in aerospace and automotive industries [7], because of its lightweight [8], low thermal expansion and good mechanical properties [9]. Due to the requirement of complex geometry they are difficult to fabricate using conventional methods. Therefore, to produce dense AlSi10Mg alloy with enhanced mechanical properties it is a good candidate for SLM. During SLM, residual stresses [10,11,12,13] generated within the part geometry that can be lead to product failure while in application, and therefore, stress relieving heat treatment cycle is a must for functional parts [14]. Post treatments [15] on aluminium alloys are performed to improve the microstructure & mechanical properties. Conventional treatments consist of heating & cooling to obtain recrystallization, microstructures during manufacturing which results in improvement of tensile properties of the alloy [16]. The aim of this review is to report a summary of the findings of various research works on the different aspects of selective laser melted AlSi10Mg aluminium alloy including process parameters, microstructure, mechanical properties and heat treatment.

 $<sup>* \ \</sup> Corresponding \ author.$ 

E-mail addresses: ravindra.gite@avcoe.org, ravigite.19@gmil.com (R.E. Gite).

<sup>&</sup>lt;sup>1</sup> Department of Mechanical Engineering, Amrutvahini College of Engineering, Sangamner, Ahmednagar, SPPU, Pune, (M.S), India.

#### 1.1. Material - AlSi10Mg alloy

The material plays an imperative role in additive manufacturing as the output quality of the product largely depends on the material characteristics and affected by powder morphology and content [17]. Till date very few materials are successfully used in additive manufacturing and proven their significance, AlSi10Mg alloy is one of them. Under the hypoeutectic aluminium alloys group, AlSi10Mg is the highly preferred material in automotive and aerospace industries due to its distinct characteristics such as excellent cast-ability, high corrosion resistance [18] and light weight [19], high dynamic load bearing capacity, good thermal and mechanical properties with higher hardness proven the better candidate for selective laser melting. Typically this alloy is used for manufacturing of cast parts having thin walls and complex geometries subjected to high loads. The parts made of this alloy can be welded, machined, wire eroded, electric discharge machined polished and coated if required [20]. The AlSi10Mg alloy falls under hypoeutectic aluminium alloys group. When the % weight of Si in Al-Si alloy is in between 11 and 13 %, the alloy is known as eutectic alloy, when the Si is less than 11 %, the alloy is known as hypoeutectic alloy and when the % weight exceeds more than 13 %, the alloy is known as hypereutectic alloy [21]. Due to the nearby eutectic configuration Al and Si, the AlSi10Mg alloys are comparatively easy to process by SLM as compared to high strength aluminium alloys but also the presence of oxides on melt pool and powder particle surface acts as a nucleation site for porosity development in selective laser melting process [22]. For the development of new alloy in SLM, the behaviour of high strength aluminium alloy has investigated to get deep insight on metallurgical aspect [23]. The Al alloys powders are highly reflective to laser beam, exhibits large heat transfer and oxidized easily, make it challenging candidate for SLM [24,25]. The AlSi10Mg alloy powder produced with gas atomization process having the particle size of 20 to 63 µm is successfully used in additive manufacturing for various applications in automotive & aerospace industries [26].

Fig. 1 shows the AlSi10Mg alloy powder morphology used for additive manufacturing. This alloy has a very small difference in solidus and liquidus temperature that enables the low tendency of cracking during solidification in SLM. The distinct microstructure and tensile properties of parts produce using this alloy can be improved by applying heat treatment. The shape and size of eutectic Si in AlSi10Mg alloy are the significant factors that affect the mechanical properties of the part [28]. The magnesium in AlSi alloy enables the Mg<sub>2</sub>Si phase in the precipitation responsible



Fig. 1. Morphology of gas atomized AlSi10Mg alloy powder [27].

for the improvement in strength and ductility without change in mechanical properties of the component [29]. The solution heat treatment (SHT) with artificial aging was used to harden the AlSi10Mg alloy. Better mechanical properties were observed in additively manufactured AlSi10Mg alloy due to the very fine structure and distribution of Si phase as compared to cast AlSi10Mg alloy [18,30].

#### 1.2. Selective laser melting (SLM)

Selective laser melting is an important and preferable AM technique used in metal additive manufacturing. In SLM, a high energy source like laser is used to melt the deposited material called substrate on the build platform. The built chamber during printing process is filled with an inert gas to avoid oxidation in melting and solidification process. The SLM involves the following important steps.

- i. A CAD model of designed component has been created and converted as.STL file.
- The generated model is oriented on build platform considering build height, surface finish and minimum support structure.
- iii. With the minimum required supports, the support structures are generated.
- iv. The CAD model file is sliced with the equal layer thickness and conveyed to printer.
- v. The build platform is preheated to lowering the heat gradient and better heat dissipation to avoid non uniform thermal expansion during SLM [31].
- vi. The layer of metal powder spread over the build platform and high intensity laser beam scan and melt the designed part geometry.
- vii. After the complete melt of one layer, the build platform lowered a distance equal to layer thickness and fresh powder again spread over the build platform. This process continues till the complete build of predefined 3D object [3].

The step vi and vii repeated till the complete build of component. The overall time required to build 3D part is categorized as primary time required for scan the powder and auxiliary time required to build platform lowering and new layer of powder deposition [3]. Basically the SLM process categorized in three distinct areas started with creating an individual scan track through laser scanning followed by formation of individual layer by joining the scan tracks and finally produces a 3D object with a layer over layer deposition [32]. During processing, the inert atmosphere is created in build chamber using Argon (Ar), Helium (He) or Nitrogen (N) to avoid oxidation effect. The parts produced in Argon environment recorded marginally higher density and mechanical properties with smoother surface as compared to Nitrogen environment and hence the type of inert gas used in build chamber didn't affect the mechanical properties [33,34]. The inert gas flow rate affects the energy density, whereas the gas pressure affects the behaviour of molten metal in SLM [35,36]. The builds quality of AM product largely affected by material properties, process parameters and working environment in SLM process [3].

#### 2. Literature review

The literature survey provides a detail summary of the findings of various research works on the different aspects of selective laser melted AlSi10Mg aluminium alloy. The SLM process is of significant intent for many researchers and has worked on various aspects like key printing parameters, optimization techniques,

R.E. Gite and V.D. Wakchaure

Materials Today: Proceedings xxx (xxxx) xxx

Materials Today: Proceedings xxx (xxxx) xxx

mechanical properties and microstructure of non-heat treated and heat treated AlSi10Mg alloy specimens. The comprehensive list of significant research is provided in Table 1.

# 2.1. SLM process parameters of additively manufactured ALSi10Mg alloy

In additive manufacturing, the printing parameters such as laser power, scan velocity, layer thickness and scan spacing are the significant parameters that disturbs the microstructure, mechanical properties and responsible for development of defects in additively manufactured product. This highlights the necessity of right selection of these parameters in SLM process. One of the common approaches to optimize these parameters is the energy density function. Table 2 presents the significant process parameters in selective laser melting.

#### 2.1.1. Laser power

The extent of energy supplied to the exposed material is controlled by the laser power in SLM [66]. The Al alloys are the highly reflective material and for such material higher laser power required for the complete melting. Incomplete melting of material in melt pool affects the melting efficiency and results in formation of defects in the final product. Laser power also affects the dimension and stability of scan track that contributes the structural integrity of the product. In SLM process the laser power significantly affects the cooling rate in melt pool. Lower laser power is responsible for the higher cooling rate in the melt pool. For the highly reflective materials, the laser power less than 200 W results in smaller size grain formation and balling phenomenon observed on the exposed surface. On the other hand, laser power over 500 W, creates lager melt pool and helps to develop larger grains. At the optimum laser power of 370 W, smoother surface with minimum satellites and increased laser energy density observed [91]. Liu et. al. [67] elaborated the influence of laser power during SLM on the grain morphology & texture in AlSi10Mg alloy. Four different levels of laser power 175 W, 225 W, 275 W, & 325 W were selected to carry out in the SLM experiments and concluded that the smaller grain size was observed for low laser power than higher one while the density increases from 97.51 % to 98.11 %, with increased laser power. Read et.al. [69] Varied the laser power from 100 W to 200 W with 25 W increments and investigated the effect on porosity development and claimed that the lower laser power results in reduction in laser energy density that causes melt pool reduction with increased porosity. Biffi et. al. [38] studied the comparative effect of continuous wave (CW) laser and pulsed wave (PW) laser on microstructure and properties of SLMed AlSiOMg alloy and reported that the dimensions of melt pool varies with the type of laser emission. The smaller heat affected zone and thinner laser tracks in pulsed laser induces better metallurgical bonding between successive layers due to lower input heat energy hence more suitable for thinner and precise structures. The rapid cooling rate in SLM develops eutectic cellular microstructure of Si surrounded by Al-Si matrix. The higher energy density of 79.12 J/mm<sup>3</sup> recorded in pulsed laser as compared to continuous

**Table 2**Selective laser melting process parameters [66].

Laser related	Powder related	Scan related	Temperature related
• Laser Power	• Particle Size	• Scan Speed	• Powder Bed Temperature
• Laser Beam Spot Size	• Particle shape & Morphology	• Scan / Hatch Spacing	• Powder Feed Temperature
<ul> <li>Pulse Duration</li> </ul>	• Layer Thickness	• Scan Pattern	<ul> <li>Temperature Uniformity</li> </ul>
• Pulse Frequency	<ul><li>Material Properties</li><li>Powder Bed Density</li></ul>		

laser those results in 50.79 J/mm<sup>3</sup>. Ding et al. [39] also concluded that pulsed laser induces higher cooling rates as compared to continuous laser.

#### 2.1.2. Scan speed

Scan speed affects the temperature in melt pool and controls the melting of material and solidification rate in SLM. Slower the scan speed, higher is the temperature in the melt pool taking longer time to solidify and cause the trapping of gases in the melt pool and results in formation of metallurgical pores. Aboulkhair et. al. [66] investigated the effect of scan speed and reported that the metallurgical pores were observed at scanning speed of 100 mm/s to 250 mm/s with increase in scan speed to 500 mm/s the metallurgical pores starts reducing and observed minimum at 1000 mm/s whereas the keyhole pores were started to develop at 500 mm/s and further increases as the scan speed increases over 1000 mm/s. These pores directly affect the porosity of final part. The higher scan speed creates balling effect that causes porosity and surface defects. Calignano et. al [115] found that the scanning speed has a significant influence on the surface roughness whereas DebRoy et al. [12] reported that the scanning speed had a significant influence on the shape and the size of the molten pool.

#### 2.1.3. Scan / hatch spacing

The scan spacing is the distance between the neighbouring layers of the built part. In SLM the scan spacing between the adjacent layers of the built part decides metallurgical bonding [66]. Higher scan spacing results in increased built in time and due to poor metallurgical bonding, the gaps started to form between the adjacent layers. Aboulkhair et. al [66] investigated the effect of hatch spacing and reported that at the minimum hatch spacing of 50 and 100  $\mu m$ , the test samples were observed to be fully consolidated even though the surface quality was poor. As the hatch spacing increase to 150  $\mu m$ , the gaps started to form between the neighbouring scan tracks. Further increase in the hatch spacing beyond 150  $\mu m$ , more gaps has been developed and balling was observed on the surface. The best results were observed when the hatch spacing was 50 or 100  $\mu m$ .

Table 1
Overview of research focus areas in additively manufactured AlSi10Mg alloy.

37,38,39,40,41,1,42,13,26,43,44, 45,46,47,48,49,50,51,52,53,54,55	<b>SLM Process Parameters</b>	Microstructure and Mechanical Pro	pperties
	Optimization	As-fabricated (Without Heat Treatment)	Post Process (With Heat Treatment)
[37,38,39,40,41,1,42,13,26,43,44,	[64,17,65,66,67,68,69,70,	[76,77,78,79,80,18,29,20,22,23,31,	[88,9,7,14,16,24,28,89,90,91,92,
45,46,47,48,49,50,51,52,53,54,55, 56,57,58,59,60,61,62,63]	71,72,12,73,74,75],	34,81,82,83,84,85,86,87,3]	93,94,95,96,97,98,99,100,101,102,103, 104,105,106,107,108,109,110,111,112,113,114

R.E. Gite and V.D. Wakchaure

Materials Today: Proceedings xxx (xxxx) xxx

#### 2.1.4. Scan pattern

The scan pattern represents the path travelled by laser beam within a layer during SLM. The common scan patterns used in SLM are meander, chequer board, strips and unidirectional [31]. The rotation and orientation of a predefined laser beam angle between the multiple layers represents the scanning strategy. It significantly affects the orientation of microstructure, pore distribution and crack formation due to residual stresses [66]. These scan designs and approaches are used to reduce the flaws and improve the microstructure. The meander and chessboard scanning strategies are most favourable in SLM. The meander strategy is suitable for thinner section parts whereas the chessboard and strips strategy used for the thicker sections. In chessboard and strips strategy, the shorter length of individual scans track helps to minimize the residual stresses developed during SLM. Qian et. al. [40] compared the effect of various scan strategies and concluded that the helix scan strategy effectively reduced the residual stresses and deformation in additively manufactured parts.

#### 2.1.5. Layer thickness

The metal powder particle size affects the layer thickness in SLM. The large particle size determines the minimal powder layer thickness. Small particles are light and get easily thrown out of the process zone, furthermore as a result of their surface to volume ratio they are more likely to inflame or explode if making contact to reactive gas. Regarding balanced particle size distribution, however, it has a positive effect on the packing density and powder compatibility as a result of small particles filling small voids. Small and narrow particle size distribution leads to uniformity in the melt pool, resulting in a higher part density [116]. Layer thickness affects the build rate, cooling rate and thermal gradient in SLM. Aboulkhair et. al. [66] studied the effect of layer thickness and concluded that with increase in layer thickness, the manufacturing time reduces but the porosity increases and results in poor surface finish and also argued that the parts produced with lower layer thickness shows better mechanical properties, higher hardness, lower surface roughness as compared to the parts produced with higher laver thickness.

# 2.2. Process parameter optimization of additively manufactured ALSi10Mg alloy

Process parameters optimization is a crucial phase in additive manufacturing as the performance characteristics of final product are mainly depends on the right selection of SLM process parameters. Aboulkhair et. al. [66] investigated the process parameters with focusing on designing the scanning strategy to improve density with minimum porosity. The samples were fabricated using scan spacing of 50 µm to 250 µm with 50 µm increment also the scan velocity increased from 250 to 1000 mm/s with 250 mm/s intervals. The laser power and layer thickness were kept constant at 100 W and 40 µm respectively. The best combination of process parameters for SLM observed was scan velocity 500 mm/s, hatch spacing 50  $\mu m$  and laser power of 100 W with a pre sintered scan strategy results in highest relative density of 99.7 %. Guan et al. [43] argued that the effect of laser power and scan velocity critically disturb the surface finish of additively manufactured parts. Calignano et al. [115] explored the effect of SLM process parameters and concluded that scanning speed significantly affects the surface quality. Kempen et al. [31] suggested optimized laser power 200 W, scan speed 1400 mm/s with 105 µm scan spacing also Brandl et al. [29] reported that laser power 250 W, scan speed 500 mm/s, scan spacing 150 μm and 50 μm layer thickness results in higher density product. Read et.al. [69] explored the effect of optimized printing parameters on defect and porosity using response surface methodology technique. Laser power, scan spac-

ing, scan speed and interaction between scan velocity and scan spacing are the significant process parameters that affect the porosity. The laser power increased from 100 W to 200 W with 25 W increments; scan velocity increased from 700 mm/s to 2000 mm/s with 350 mm/s increments and scan spacing increased from 30 µm to 120 µm with 22.5 µm increments. The porosity increases due to increased scan speed and decreased laser power as both the parameters ultimately affects and reduces the energy input to the material and results in melt pools reduction and cause increase in porosity. Bai et. al. [73] highlighted the influence of SLM parameters on microstructure and tensile properties of non-heat treated and heat treated AlSiMg0.75 alloy. The response surface method technique was used to optimize important SLM parameters like laser power scans speed, hatch spacing and layer thickness. The higher scan velocity with low laser power causes unmelt powder results in decrease in relative density, whereas higher laser power with slow scan speed also results in low relative density due to formation of spatters and voids. The higher relative density of 99.06 % was observed at the laser power of 179 W; scan velocity of 647 mm/s and hatch spacing of 105 μm. Superfine cellular and dendritic grain microstructure was observed in asfabricated samples due to the higher cooling rate in printing. After applied heat treatment of 300 °C for 2 h, the developed cellular and dendritic grain microstructure breaks and reduction in mechanical properties observed. Majeed et. al. [74] investigated the effect of laser power, scan velocity, hatch spacing and overlap rate in SLM. The full factorial methodology with ANOVA and regression analysis was used for process parameters optimization. The laser power increased from 320 W to 400 W with 40 W increments, scan velocity increased from 600 mm/s to 900 mm/s with 150 mm/s increments and scan spacing improved from 70 µm to 116 µm. The best surface quality of as fabricated samples was observed at laser power of 320 W, scan velocity of 600 mm/s, 88.7 µm hatch spacing and 35 % overlap rate. The average surface roughness of heat treated samples at 540 °C for 2 h initially decreases and increased after aging at 155 °C for 12 h. Anwar et. al. [75] elaborated the effect and interaction of inert gas flow velocity, scan direction and part. The inert gas velocity of 30 % (1.47 m/s) and 60 % (2.87 m/s) of maximum velocity was set as input parameters in SLM. Irrespective of part placement and gas velocity, the aligned laser scans direction along with inert gas flow significantly decreases the powder accumulation near the outlet and observed fine particles in the laser beam path. Better part quality was observed with higher gas velocity, but increasing gas velocity swipes the fresh power from powder bed. Wang et al. [33] concluded that the part density and hardness was not affected by the type of inert gas used in SLM. Liu et. al. [64] identified the effect of laser powder deposition parameters and investigated the optimized parameters to achieve maximum density of build part. The Taguchi technique with ANOVA was used for optimization as it was proven useful to investigate multiple parameters effect in complex object. The controllable parameters such as laser power, scan speed, shielding gas flow rate and powder feed rate with five levels were selected for the experimentation. The laser power varied from 120 W to 160 W with 10 W increments, scanning speed varied from 400 mm/min to 600 mm/min with 50 mm/min increments. The powder feed rate increased from 0.66 g/min to 0.9 g/min with 0.06 g/min increments and the shield gas flow rate increased from 6 L/min to 8 L/min with 0.5 L/min increments. The optimized process parameters after experimentation were laser power 150 W, scan speed 400 mm/min, shielding gas flow rate 0.78 g/min and powder feed rate 7 L/min. Laser power and scan speed are the dominant factors that contributes 49.43 % and 33.74 % respectively to relative density. The relationship between relative density and energy density investigated to achieve higher densification. Trevisan et. al. [115] reviewed & summarized the effects of the printR.E. Gite and V.D. Wakchaure

Materials Today: Proceedings xxx (xxxx) xxx

ing parameters on the properties of the output parts starting from the powder characteristics to the printing parameters. The collective effect of printing parameters evaluated using energy density [89 81] and also highlighted the applied heat treatments established for conventionally fabricated materials & applied on 3D printed materials. The orientation modifies the microstructural growth of the material, and introduces defects & anisotropy. Wang et al. [24] examined the effect of laser energy density on quality of additively manufactured AlSi10Mg alloy and reported that surface quality improved with increase in laser energy density.

#### 2.2.1. Laser energy density

The laser power is the significant parameter, as it affects the degree of consolidation of the material powder, and advances the defect formation by developing turbulences in the melt pool that causes defect in the part. The popular approach to characterize the laser power is the energy density function  $(\Psi)$  [69,3,67,110,115,90,91,24,44]. The normally used energy density function suggested in the literature is volumetric energy density (I/mm³) [45] & calculated as follows:

$$\psi = \frac{P}{V * H * T} \tag{1}$$

Where P is laser power (W), V is scan velocity (mm/s), H is hatch spacing ( $\mu$ m) and T is layer thickness (mm).

The porosity is largely affected by laser power, scan velocity and the interface between the scan velocity and scan spacing. In order to reduce or eliminate the porosity from the material, a higher laser power with a slower scan velocity with minimum scan spacing should be used. Yang et al. [37] evaluated the influence of laser energy density on surface irregularity and morphologies of SLM produced AlSi10Mg parts. The lower laser energy density was responsible for incomplete spread of molten pool due to the short solidification time that results in insufficient penetration of energy in the powder layer that initiated to develop the balling phenomenon on the surface [117]. The suitable laser energy density with enough solidification time allows molten metal to spread in melt pool with decrease in the Marangoni convection and causes smoother surface. When the laser energy density was set in between 4.625 J/cm to 7.4 J/cm, the measured surface roughness was under 6 µm. The higher laser energy density results in stronger Marangoni convention with metal evaporation, causes instability of deposited tracks and increase in surface roughness. Wang et al. [24] elaborated the effect of laser energy density on surface quality of additively manufactured AlSi10Mg alloy and reported that surface quality improved with increase in laser energy density. Hirata et. al. [110] explored the effect of porosity and energy density on microstructure and tensile properties of as fabricated and hot isostatic pressing (HIP) heat treated AlSi10Mg specimens. The specimens were heated at 500 °C for 2 h. Fine dendritic cell microstructure was observed in as-fabricated samples whereas in heat treated specimens the Si diffused and coarse granular phases were observed. The higher cooling rate in SLM, initiates the  $\alpha$ -Al phase and heterogeneous nucleation process proceeded with elimination of Si and Mg that further solidified to form the crystallized phase. As the energy density decreases, the amount and size of internal pores increases that affects the mechanical properties of the specimen therefore highlighted the importance of optimization of laser irradiation condition in SLM process.

Table 3 presents the key published literature on additively manufactured AlSI10Mg alloy including the SLM system used, process parameters selected and important findings. It was observed that most of the investigators used commercial SLM system developed by foremost SLM manufactures such as Renishaw, SLM Solutions, Realizer GmbH and Concept laser.

From the detailed study of the above literature, following ranges of the SLM process parameters for additively manufactured AlSi10Mg alloy are suggested in Table 4.

$$Scan Speed (mm/sec) = \frac{Point \, Distance \, (mm)}{Exposure \, Time \, (sec)}$$

#### 2.3. Microstructure of AlSi10Mg alloy

The microstructure of the printed components is the end result of alloy powder melting, solidification during SLM and post heat treatment. For the additively manufactured samples a different microstructure is obtained due to the different manufacturing method. The rapid solidification [120] caused by SLM is responsible for the fine microstructure and this fine microstructure is the reason for the high mechanical properties [66]. Aboulkhair et. al. [66] revealed that two different forms of microstructure observed in SLM samples. The fine microstructure observed at the core of melt pool whereas the coarse dendritic microstructure with elongated grains observed at the borderline of melt pool. The coarsening of grains is due to the slower solidification rate in the boundary region as compared to the core. Thijs et al. [31] highlighted that the melt pool consist of fine microstructure at core and coarse microstructure towards the boundary region and heat affected zone. Trevisan et. Al [115] reviewed and summarized that the unique microstructure observed due to the cyclic melting and fast cooling of powder material in SLM. Lam et. al. [82] observed the cell like dendritic structure of  $\alpha$ -Al and eutectic Si phase network along the  $\alpha$ -Al boundary with the dimensions of 500 to 1000 nm. Prashanth et. al. [85] revealed that the solidification of  $\alpha$ -Al into cell like morphology and prolonged solubility of Si into Al observed during SLM process. The remaining Si was observed at the cell like boundaries having a thickness of 200 nm. The scanning strategy and process parameters significantly affect the microstructure in SLM process. Rosenthal et al. [86] reported that the developed thermal gradient (G) and growth rate (R) critically affects the solidification rate in SLM process. The growth rate can be controlled by changing scan speed and laser scan angle during processing. The cooling rate was calculated by multiplying thermal gradient and growth rate. The increased growth rate results in formation of cellular structure [121] that finally converted into dendritic morphologies. Maximum thermal gradient and growth rate were observed near the centre of melt pool and reduces towards the border. Brandl et al. [29] elaborated the consequence of post process heat treatment on microstructure and showed that the cell like α-Al dendritic structure and Si particles in in-built phase were modified and globular Si particles distributed evenly inside the  $\alpha$ -Al matrix. Liu et. al. [76] highlighted the effect of cooling rate on the formation of microstructure and tensile properties during SLM. The FEA model was used to calculate the cooling rate of melt pool. Also the Si particle distribution and size, dendrites and sub boundaries were analysed. The melt pool was divided into core and surface regions. The higher cooling rate of  $1.44 \times 10^6$  K/s observed in the surface region as compare to core with cooling rate  $\leq 1 \times 10^3$  K/s. The surface area with higher cooling rate consist of fine Si particles, more sub boundaries and dendritic structure results in higher hardness and good wear resistance. The dendritic structure of  $\alpha$ -Al phase and inter dendritic Si particles were observed in the microstructure.

Fig. 2 shows a microstructural development mechanism in the heat treatment. Initially the microstructure was contains a eutectic Si and primary  $\alpha$  phase. The irregularly shaped Si particles are spread along the grain boundaries. During heat treatment, the Si particles were decomposed at a relatively high temperature and dissolved in the  $\alpha$ -Al matrix to form uniform microstructure. The

**Table 3**Summary of SLM process parameters and research findings of AlSi10Mg Alloy.

Author	SLM System		SLM Pr	rocess Parameters				Research Findings	Ref.
(Year)			Laser Power	Scan Speed	Hatch Spacing	Layer Thickness	Scan Strategy		
Kempen et. al. (2012)	Modified Concept Laser M1, 200 W fibre las 150 $\mu m$	er, beam dia.	200 W	1400 mm/s	105 μm	-	-	<ul> <li>Better Mechanical properties observed in AM AlSi10Mg as compared to cast AlSi10 Mg due to fine microstruc- ture.</li> <li>Some anisotropy in elongation observed in AM samples.</li> </ul>	[18]
Brandl et. al. (2012)	Trumpf Truma Form LF130 powder-bed ma YAG laser laser – 250 W laser beam spot di Inert gas - Argon		250 W	500 mm/s	150 μm	25 μm	-	• The microstructure of as-built samples is characterized by cell like dendrites of $\alpha$ -Al and inters dendritic Si particles.  The combinations of 300 °C platform temperature and peak hardening are a better combination to improve fatigue resistance.	
Aboulkhair et. al. (2014)	A Realizer GmbH SLM 50,Germany, yttrium 100 W	fibre laser –	100 W	250 mm/s, 500 mm/ s, 750 mm/s, 1000 mm/s	50 μm 100 μm 150 μm 200 μm 250 μm	50 μm	Uni- directional	<ul> <li>The pores developed in SLM are related to scanning speed.</li> <li>Smaller hatch spacing gives the better results.</li> <li>Two types of microstructure, fine at center and coarse structure at boundary, observed in, melt pool.</li> </ul>	
Buchbinder et. al. (2014)	EOSINT M 270		195 W	800 mm/s	150 μm	30 μm	_	<ul> <li>With the preheated build plate, decrease in hardness with better crack resistance observed.</li> <li>Lower temperature gradient developed in preheating, results in lower thermal stresses.</li> </ul>	[46]
Mauduit et. al. (2015)	Phenix Systems PM100, fibre laser YAG 200 v Argon	W. Inert gas -	200 W	700 mm/s	-	30 μm	Crossed	<ul> <li>Substantial increase in the mechanical properties of SLM AlSI10Mg as compared to casting due to microstructure refinement.</li> <li>Due to the residual stresses, it is difficult to produce</li> </ul>	
Aboulkhair et. al. (2015)	Realizer GmbH SLM-50 (Germany), 100 W Maser, laser beam spot dia. $-20~\mu m$ , Inert g.		100 W	250-1500 mm/s	50 μm	40 μm & 400 μm	-	<ul> <li>metal matrix samples with 15 % SiC reinforcement.</li> <li>With increase in laser scan velocity, the dimensions of melt pool decreased.</li> <li>As layer thickness increase, the defects like satellites, discontinuities, irregularities and balling increases.</li> </ul>	[48]
Author	SLM System	SLM Process	Parameters					Research Findings	Ref.
(Year)		Laser Power	· So	can Speed	Hatch Spacing	Layer Scan Thickness Strategy			
Read et. al. (2015)	Concept Laser M2 system, Yb-Fibre laser – 200 W, laser scan velocity – 7000 mm/s, spot dia. – 150 µm	100 W, 125 Y 150 W, 175 Y 200 W	W, 13	00mm/s, 1025 mm/s, 350 mm/s, 1675 mm/s, 000 mm/s	30 μm, 52.5 μm, 75 μm, 97.5 μm, 120 μm	30 μm	Chequer Board (Island)	<ul> <li>The build direction does not affect mechanical properties and creep strength of SLM samples.</li> <li>Un-melted powder observed on the fracture surface that initiates the crack propagation in SLM samples.</li> </ul>	[69]
Aboulkhair et. al. (2020)	Renishaw AM 250 SLM machine, 200 W Yb-Fibre laser	200 W	57	70 mm/s	130 μm	25 μm	Checquer board	A Higher micro hardness of 109.7 HV observed in the plane parallel to build plate than perpendicular plane.  Due to homogeneous distribution of Si particles, uniform Nano-hardness was observed.	[42]
Lam et. al. (2015)	SLM280HL machine, laser beam spot size dia. – 80 μm	350 W	93	30 mm/s	190 μm	50 μm	-	• The microstructure of as-fabricated part was cell like dendrites of $\alpha$ -Al phase and eutectic Si with Mg <sub>2</sub> Si phase.  The gained cell like dendritic $\alpha$ -Al phase dissolved a small content of Si and developed the face-centre cubic Al.	[82]
Beretta et. al. (2020)	SLM 280HL SLM Solution Group AG, Inert gas - Argon	350 W	16	650 mm/s	130 μm	50 μm	Strips	<ul> <li>The specimen built in XY direction exhibits higher fatigue strength as compared to vertically built spec- imens.</li> </ul>	[62]

Table 3 (continued)

	LM System	SLM Pr	ocess Pa	rameters					Research Findings	Ref.
(Year)		Laser P	ower	Scan Speed	Hatch	Spacing	Layer Thickness	Scan Strategy		
									Reasonable correlation between surface roughness and crack development was observed in the printed parts.	
	enishaw AM 250 SLM machine, 200 W Yb- ibre laser	200 W		570 mm/s	130 µг	n	25 μm	Chequer board	• The SLM pares had better mechanical strength as compared to cast parts.  The YS of heat treated samples was observed 169 MPa which was less than as-fabricated samples.  The harness and tensile strength reduced to 20 % and 12 % respectively after heat treatment, whereas ductility increased by 2.8 %.	[111]
Aboulkhair R et. al. (2016)	enishaw AM250	200 W		570 mm/s	80 μm		25 μm	Chessboard	<ul> <li>As-built samples show good performance under cyclic loading.</li> <li>Heat treatment significantly improves the fatigue life of printed part.</li> </ul>	
•	oncept Laser M2 Cusing system, Yb-fibre aser – 400 W, laser beam dia – 60 μm	175 W		1025 mm/s	97.5 μ	m	30 μm	Island	<ul> <li>Post processing using T6 and HIP develops a homogeneous microstructure with Si particles in Al matrix.</li> <li>Horizontally built samples shows better mechanical properties as compared to vertically built samples.</li> </ul>	[93]
Author (Year)	SLM System		SLM Pro	ocess Parameters				Research	Findings	Ref.
			Laser Power	Scan Speed	Hatch Spacing	Layer Thickness	Scan Strategy			
SLM 250 HL SLM Solutions GmbH, Gaussian beam fiber laser – 400 V spot dia. – 80 µm  Anwar et. al. 280 HL (SLM Solutions Germany),		-	350 W	1140 mm/s	170 μm	50 μm	-	decrea The si of sai	e temperature increases, the solubility of Si particles in Alases. ze of Si particles significantly affects the tensile properties mples, as the size increases the mechanical strength ases from 434.25 to 168.11 MPa for as-built samples.	
Anwar et. al. (2017)	spot dia. — 80 μm ar et. al. 280 HL (SLM Solutions Germany), twin		350 W	900 mm/s	120 μm	-	-	<ul> <li>Spatte prope Scann</li> </ul>	ering is an unavoidable phenomenon in SLM that affect the rties of printed part.  ing in the gas flow direction significantly reduces the accuion the spattered powder near the outlet.	[75]
Hitzler et. al. (2016)	280HL, SLM Solutions GmbH, German W Yb-fiber-laser, Inert gas - Nitrogen		350 W	930 mm/s	420 μm	50 μm	-	<ul> <li>The harmonic face in No sign</li> </ul>	ardness deviation and rupture observed at the upper surn n SLM samples. gnificant effect observed of Nitrogen as inert gas on proper- f SLM samples.	[41]
Fiocchi et. al. (2016)	Renishaw - AM 250, Inert gas - Argor spot size dia. – 130 μm	n, laser	300 W	1083 mm/s, (Exposure Time – 120 μs, Point Distance – 130 μm.)	140 μm	25 μm	-	<ul> <li>The Si tempe</li> </ul>	i network remains unchanged during lower heat treatment erature. i transformation takes place after 294 °C in annealing heat	
Ding et. al. (201	6) Renishaw AM250, laser beam spot dia μm, Inert gas - Argon	a 135	400 W	1000 mm/s, (PW - Exp. Time – 130 μs, Point Dist – 130 μm.)	135 μm	25 μm	-	<ul> <li>Under cal sh shows</li> </ul>	r same energy input, the point exposure laser show ellipti- aped molten pool, whereas the continuous exposure laser s comet shaper molten pool. exposure laser fine grains obtained due to higher cooling	
Maskery et. al (2016)	Renishaw AM250 SLM machine, Yb fil laser (wavelength 1070 nm), Inert gas Argon		200 W	571 mm/s (Point Dist – 80 μm, Exposure time – 140 μs)	130 μm	25 μm	Meander	<ul> <li>A SLM energy There</li> </ul>	If with post processing can be used to produce lightweight y absorbing structures.  is restriction of the Gibson-Ashby based analysis as ed to graded density structures.	
Wang et. al. (20 <sup>-</sup>	17) SPI+ SCANLAB system, Yb fibre laser, beam diameter – 70 μm, Inert gas - A		215 J	500 mm/s	70 μm	25 μm	Chessboard & Linear	d • Laser micro The vi	parameters significantly affect the growth direction of structure. ibration testing proved that the AM parts showed better e properties and fulfil the requirements of aeronautical	

Author	SLM System	SLM Pro	rocess Parameters					Research Findings		
(Year)		Laser Power	S	can Speed	Hatch Spacing	Layer Thickness	Scan Strategy			
Zhuo et. al. (2017)	SLM 280 HL AM system, 400 W fiber laser, laser beam dia. $-$ 80 $\mu m$	300 W	8	00 mm/s	130 μm	30 μm	=	<ul> <li>The heat treatment at 300 °C for 2h with water quenching is effective to reduce residual stresses.</li> <li>The residual stresses were reduced to -13 MPa from -111 MPa.</li> </ul>	[16]	
Takata et. al. (2017)	EOSINT M 280 AM system, Yb laser — 380 W EOS GmbH, Germany.	380 W	-		100 μm	30 μm	-	<ul> <li>The melt pool consists of columnar α-Al surrounded by superfine Si particles.</li> <li>At higher temperature coarse Si particles were observed with a stable intermetallic phase.</li> </ul>	[88]	
Trevisan et. al. (2017)	-	20 W, 2 W		0 mm/s, 50 mm/s	100 μm		-	<ul> <li>For each metal powder the process parameters should be optimized correctly.</li> <li>In as-fabricated samples higher mechanical properties and more residual stresses were observed.</li> <li>Need to develop new heat treatment process to improve mechanical properties.</li> </ul>	[115	
Liu et. al. (2018)	BLT-S300 SLM machine, Xi'an Bright Additive Technologies Co., ltd.	500 W	1	500 mm/s	-	30 μm	Zig-Zag	<ul> <li>The higher cooling rate of 1.44 x 10<sup>6</sup> K/s observed at the upper surface as compared to lower surface of 1 x 10<sup>3</sup> K/s in SLM.</li> <li>Higher cooling rate in top surface of melt pool develops sub grains and sub boundaries and fine Si particles.</li> <li>The fine Si particles results in higher hardness and wear resistance in SLM samples.</li> </ul>	[76]	
Raus et. al. (2017)	SLM 125 HL, SLM Solutions, fibre laser 400 W laser beam spot dia. $-$ 80 $\mu$ m, Inert gas - Argon	350 W	1	650 mm/s	130 μm	30 μm	Strips	<ul> <li>SLM shows very high values of UTS, YS, hardness &amp; % elongation at break as compared to HPDC alloy A360F and A360T6.</li> <li>Relative density of 99.3 % achieved with low porosity.</li> </ul>	[77	
Salmi et. al. (2017)	SLM EOSINT M 270 extended machine, Inert gas – 120 W Argon, laser spot size dia. – 10 μm W, 80			00 mm/s, 00 mm/s	100 μm, 170 μm	30 μm	Island	<ul> <li>The direct contact between print sample and support structure has significant effect on residual stresses.</li> <li>The standard heat treatment adopted not sufficient to relive residual stresses.</li> </ul>	[68	
Tang et.al. (2017)	EOS M280 SLM machine, laser beam spot dia 100 $\mu m, $ 370 W Inert gas - Argon		1	300 mm/s	220 μm	30 μm	-	The Z oriented samples show smaller tensile ductility as compared to XY oriented ductility. The porosity also affects the tensile ductility.	[50	
Author	SLM System		SLM Pı	ocess Para	neters			Research Findings	Ref	
(Year)			Laser Power	Scan Speed	Hatch Spacing	Layer Thicknes	Scan s Strateg	y		
Pei et. al. (2017)	Self-developed SLM 150, ytterbium fiber laser YLR-500-Y11, IPG, Laser Gmbh, Germany, laser beam dia $-$ 70 $\mu$		150– 180 W	600– 1400 mm/s	50 μm, 60 μm, 70 μm	40 μm	Randor rotation		[78	
Palumbo et al. (2017)	EOSINT M280, Yb fiber laser 400 W, Beam wavelength: 1100 nm, laser beam dia. – 100 μm	: 1060–	400 W	7000 mm/s	-	-	-	<ul> <li>The use of smaller layer thickness and hatch distance results in higher density and mechanical properties.</li> <li>The higher scan speed results in tighter and cleaner welding beds within the sintered material.</li> </ul>	[51	
Chen et. al.	SLM 250HL, SLM Solutions Germany, yb fiber laser, lase	er beam	350 W		240 μm	50 μm	-	• The higher YS of 300 MPa and UTS of 455 MPa observed.	[52	
(2017) Boschetto et. al. (2017)	dia – 0.08 mm EOSINT M systems, EOS GmbH – Electro Optical Systems, beam dia. 100 μm		370 W	mm/s 1300 mm/s	0.19 mm	30 μm	-	<ul> <li>Higher strength and strain hardening due to Orowan looping.</li> <li>The balling effect was developed due to the satellite particles and staircase effect in feedstock powder.</li> </ul>	[11	
Xiong et. al. (2019)			350 W	920 mm/s	-	-	-	$ \bullet \  \   \hbox{Columnar} \ \alpha-\hbox{Al grains observed with cell like structure in eutectic Si \& \hbox{Al matrix.} \\ \  \   \hbox{Crack initiated and progressed along the melt pool boundaries.} \\ \  \   \hbox{The anisotropy in samples was governed by spreading of melt pool boundaries on surface.} \\ \  \   \hbox{Columnar} \  \   \   \   \   \   \   \  $	[83	

 $\infty$ 

Table 3 (continued)

Author	SLM System	SLM	Process Pa	rameters				Research Findings	Ref.
(Year)		Lase Pow		Hatcl Spaci		Layer Thickness	Scan Strategy	-	
Liu et. al. (2018)	EOSINT M 280 SLM system, EOS Germany – Yb fiber laser, Ir gas - Argon	nert 380	W 1000 mm/s	-	3	30 μm	Meander	<ul> <li>The microstructural change is due to the solidification direction in SLM.</li> <li>The melt pool consists of columnar α-Al phases surrounded by fine eutectic Si particles.</li> </ul>	[79]
Casati et. al. (2018)	EOS M290 SLM system	340	W 1300 mm/s	200 ֈ	ım 3	30 μm	-	<ul> <li>The conventional T6 heat treatment results in poor mechanical strength with improved ductility.</li> <li>SLM parts produced on cold platform results in improved mechan- ical properties as compared to parts printed on hot platform.</li> </ul>	[53]
	SLM System	SLM Pr	ocess Para	meters			Re	esearch Findings	Ref.
(Year)		Laser Power	Scan Speed	Hatch Spacing	Layer Thicknes	Scan ss Strate	gy		
-	Renishaw AM 250 system, ytterbium fiber laser $-$ 400 W, laser beam dia $-$ 76 $\mu m$ , lnert gas - Argon	400 W	1000 mm/s	175 μm	25 μm	Chessl or Isla		<ul> <li>T6 HT has no significant effect on part densification. Similar densification of 96 % &amp; 96.52 % was observed in as-fabricated and post processed samples.</li> <li>20 % hardness reduced in heat treated samples as compared to as-built samples.</li> </ul>	[24]
Fousova et. al. (2018)	SLM Solution 280 HL machine, 400 W YLR-Faser-Laser	350 W	500 mm/s	170 μm	50 μm	-		T6 HT improves fracture toughness.  • At 160 °C temperature, improvement observed in tensile and yield strength but reduces % elongation.  Conventional heat treatment results in significant drop in mechanical properties.	[9]
Girelli et. al. (2019)	EOS M290 system, Yb fibre laser – 400 W, beam dia 100 μm	1 370 W	1300 mm/s	190 μm	30 μm	-	•	<ul> <li>As-built AM parts exhibits superior mechanical properties as compared to gravity cast produced parts due to grain refinement.</li> <li>For both GC &amp; AM samples, better performance observed after HT at 540 °C for 1h, water quenching followed by ageing at 180 °C for 1h.</li> </ul>	[94]
0	Concept Laser M2, Yb-fiber laser — 400 W, laser beam dia — 50 µm, wave length range is 1064–1100 nm, Inert gas - Argon		1500 mm/s	105 μm	50 μm	-	•	<ul> <li>As laser energy density increases, the stability of deposited tracks decreases.</li> <li>With lower laser energy density, the balling phenomenon's observed in melt pool.</li> </ul>	[37]
Maamoun et. al. (2018)	EOS M290 machine, 400 W Yb-fiber laser, Inert gas - Argon	370 W	1300 mm/s	0.190 mm	30 μm	Strips	•	Recycled powder can be reused to reduce cost.     Similar microstructure was observed in recycled powder.     Higher relative density of 99.7 % observed.	[95]
Lv et.al.	Raycham LDM 8060, 4 kW Laserline IPG fibre laser, Inert gas - Argon	2000– 3600 W	360– 840 mm/s	150 μm	-	'S' stra	itegy	9	[96]
Author (Year)	]	Laser S	ess Paramet Scan Speed	ers Hatch Spacing	Layer Thickn	Scan ess Strat	Į.	Research Findings	Ref.
Sajadi et. al. (2021)	TruPrint 3000 machine (TRUMPF GmbH + Co. KG, Ditzingen, BW, Germany)		1300 mm/ s	210 μm	50 μm	Ches	sboard	After the heat treatment, columnar dendritic sub grains, and hatch	[97]
Mertens et. al. (2015)	. MTT SLM 250	175 W	195 mm/s	190 μm	60 μm	-		overlaps, disappear.  • Better Mechanical properties were observed after heat treatment at 250 °C, 2h.  The hardness of as-fabricated samples observed more than heat treated samples	[98]
Zhang et. al. (2019)	Self-developed machine (LSNF-2)		2000 mm/ s	100 μm	40 μm	Zig Z	'ag	*	[99]
Krishna et. al. (2020)	EOSINT M 280, 400 W Gaussian beam fiber laser, beam diameter — 80 μm, Inert gas- Argon	350 W	1140 mm/	170 μm	50 μm	_			[84]
Takata et. al.		380 W	_	150 μm	30 μm				[80]

Table 3 (continued)

Author (Year)	SLM System	Sl	· · · · · · · · · · · · · · · · · · ·					dings	Ref	
			aser Ower	Scan Speed	Hatch Spacing	Layer Thickness	Scan Strategy			
(2018)								• The alloy	hardness marginally reduced with reducing sample width.	
Fang et.al. (2016)	EOS M280, Laser beam diameter – 80 μm	3	70 W	1300 mm/	190 μm	30 μm	-		pool consist of columnar $\alpha\text{-Al}$ grains enclosed by Si particles atch spacing & build orientation affects mechanical properties	[54
` ,	Concept Laser M2 Cusing machine	20	00 W	1400 mm/ s	97.5 μm	30 μm			stresses reduced approximately by 20 %. Icture restructured after T6 heat treatment.	[1
Ding et. al. (2017)	_	4	00 W	300 mm/s	130 μm	-	-	<ul> <li>Exposure</li> </ul>	time has insignificant effect on heat transfer. cance affects width & depth of melt pool.	[5
	Trumpf Trumaform LF250 machine, Nd:YAG lase 1000 W	r – 9	10 W	1000 – 4000 mm/ s	200 μm	50 μm	_		OMg alloy powder required to reduce porosity. speed lead to outgassing of pores from the melt pool.	[5
luthor (Year)	SLM System	SLM Pro	ocess Pa	rameters					Research Findings	Re
		Laser Power	Sca	n Speed		Hatch Spacing	Layer Thickness	Scan Strategy		
arrosa et. al. (2018)	Concept Laser M2 Cusing system, Ytterbium fiber laser — 400 W, spot size dia. — 60 µm, Inert gas - Argon	175 W	102	25 mm/s		97.5 μm	30 μm	Chequer Board (Island)	• In SLM, micro porosity formed due to lack of fusion, shrinkage and gas evolution during solidification process.  To heat treatment followed by HIP reduces porosity during built.  The yield strength of as-built samples observed better.	[5
/ang et. al. (2018	S) Space M200 type SLM	200 W, 300 W, 400 W	100 mn	0 mm/s, 200 i n/s	mm/s, 300	150 μm	50 μm	-	The residual stresses can be controlled by influencing the temperature field in melting and solidification of powder layer.     In SLM process, the laser power affects the energy input, the scanning speed affects the cooling rate, and the laser scanning strategy affects the heat dissipation.	[7
iffi et. al. (2018)	Renishaw AM 250 system, Pulsed Wave (PW) ytterbium fiber laser; SLM 500 system, 400W Continuous Wave (CW) fiber laser	PW – 300 W, CW – 350 W	Tin	66 mm/s, (PW ne – 120 μs, I ) μm.) CW –	Point Dist –	PW — 140 μm, CW — 170 μm	PW – 25 μm, CW – 50 μm	-	<ul> <li>In continuous wave laser samples, the Mg<sub>2</sub>Si precipitation was trigged whereas pulsed wave laser are characterized by lower activation energy related to Si precipitation.</li> <li>The obtained energy densities were 50.79 J/mm³ for the CW sample and 79.12 J/ mm³ for the PW sample.</li> </ul>	[3
mani et. al. (2018)	SLM 250, Inert gas - Argon	250 W	<b>57</b> 1	l mm/s		-	60 μm	-	<ul> <li>A FEA model was developed for analysis.</li> <li>Simulation revealed the similar agreement with developed models prediction of fracture.</li> </ul>	[5
rurrioz et. al. (2018)	SLM 280HL	400 W	-			-	-	-	<ul> <li>The relative density of 99.9% was observed in as-fabricated samples. After heat treatments, due to the formation of Si, the tensile strength and hardness reduced.</li> <li>To heat treatment was found best performing heat treatment.</li> </ul>	[1
Han et. al. (2018)	AM250 Renishaw plc, Wotton-under-Edge, Gloucestershire, UK,SLM system, ytterbium fiber laser	200 W	500	) mm/s		130 μm	25 μm	chessboard fill-hatch type	Heat treatment does not have significant effect on surface finish.     Tensile properties can be tailored by controlling the post process heat treatment parameters.     The high-frequency laser surface remelting enhanced the micro hardness.	[1
	System	SLI	M Proce	ess Paramete	ers				Research Findings	Re
Year)		Las	ser Pow	ver Scan	Speed	Hatch Spacing	Layer Thickness	Scan Strategy		
Asgari et. EOS	M290 machine, Yb-fiber laser –400 W, laser bea	m 27	0 W	1300		170 μm	90 μm	Strips		[5

Table 3 (continued)

Author	SLM Sys	stem	5	SLM Process P	arameters				Research Findings	Ref.
(Year)			Ī	Laser Power	Scan Speed	Hatch Spacir		Scan Strate	ey	
(2017)									<ul> <li>As the strain rate increased from 150/s to 1600/s, the improvement in stress and ductility observed.</li> <li>The texture is not affected by deformation of high strain rate.</li> </ul>	
Liu et. al. (2019)	TRUMP	F Trumaform Lf 250 machine, Spot dia		175 W, 225 W, 275 W, 325 W	-	-	-	Strips	<ul> <li>Both columnar and equiaxed grains were observed in SLM samples.</li> <li>The grain size is much smaller in low laser power samples.</li> </ul>	
Bao et. al. (2020)		0 (Xi'an Bright Laser Technologies Co., ltd er, Inert Gas - Argon	1), 500 W 3	360W –400W	1200mm/s – 1500 mm/s	130 μι – 160 μm		-	<ul> <li>Cyclic plasticity observed when strain exceeds 0.9.</li> <li>The development of flaws along the loading direction is 10 times greater than that of lateral side.</li> </ul>	[72]
Liu et. al. (2019)		w AM 400, modulated ytterbium fibre la ngth- 1070 nm, spot dia – 80 μm	aser, 2	200 W	-	80 μm	n 25 μm	Meander, Strips, Chessboard	<ul> <li>The laser remelting effectively improves the surface roughness &amp; relative density up to 99.3 %</li> <li>The fine grains with supersaturated α-Al improve the hardness from 117 HV to 121 HV.</li> </ul>	
Dong et. al. (2019)		90 Machine, Yb-fiber laser —400 W, bea m, Inert gas - Argon	m dia. 3	370 W	1500 mm/s	150 μι	m 30 μm	-	<ul> <li>As the build angle increased from 35.5° to 90°, the overall mechanical properties improves more than 12 %.</li> <li>The cooling rate in upper surface is twice as that of</li> </ul>	
Jiang et. al. (2019)	Space M	1200 Machine	4	400 W	200 mm/s	150 μι	m 50 μm	Chessboard	<ul> <li>lower surface.</li> <li>The stress &amp; strain variation observed with variation in heating temperature.</li> <li>Heating temperature of 350 °C is more suitable for SLM samples.</li> </ul>	
Zhang et. al. (2019)		eloped multi-laser beam SLM system,4 l laser spot size dia. – 100 μm, Inert gas		490 W	1800 mm/s	100 μι	m 40 μm	Raster	The microstructure of overlap area is slightly different than isolated area.     The isolated and overlap samples shows similar microstructure and mechanical properties.     The cracks mainly developed along the melt pool boundaries.	
Majeed et. al. (2019)	SLM 280	O HL machine		320 W, 360 W, 400 W	600 mm/s, 750 mm/s, 900 mm		30 μm	-	As the laser power increases, the surface roughness increases due to increased laser beam intensity.     As the scanning speed of laser beam increases, surface roughness initially decreases and the slightly increases.	
Author (Yea	ar)	SLM System	SLM Proce	ss Parameters	;			R	esearch Findings	Ref.
			Laser Pow	er Scan Sp	eed	Hatch Spacing	Layer Thickness	Scan Strategy		
Parveen et. (2021)		SLM 280HL system, Ytterbium fiber laser – 400 W, laser spot size 80 µm	170–250 V	V 500–700	mm/s	-	35 μm, 60 μm	-	<ul> <li>With increase in layer thickness, the build time can be reduced, that reduces the production cost.</li> <li>Better mechanical properties were observed for lower layer thickness.</li> </ul>	
Hirata et. al. (2019)		EOSINT M280 EOS GmbH, Yb fiber laser – 400W, laser beam dia. – 100 μm, Inert gas - Argon	300 W	1200 mi	m/s	150 μm	-	-	<ul> <li>Hot Isostatic Pressing (HIP) heat treatment results in fine dendritic cell microstructure of sub-micron size were observed.</li> <li>No major changes were observed in different energy densities.</li> </ul>	[110]
Liu et. al. (2	,	Laser powder Deposition system, Laser power – 500 W, Beam diameter – 0.5 mm	120 W, 130 W, 140 W, 150 W, 160	min 500	/min 450 mm/ mm/min 550 a 600 mm/min	-	-	-	<ul> <li>Laser power is the most significant parameters in SLM that contributes 49.43 % in relative density followed by scan speed that contributes 33.74 %.</li> <li>Almost fully dense part obtained under the optimized process parameters.</li> </ul>	
Ch et. al. (20	,	EOS M280 DMLS machine, Inert gas - Argon & Nitrogen	370 W	1300 mi	m/s	190 μm	30 μm	-	parameters.	[119]

Table 3 (continued)								
Author (Year)	SLM System	SLM Process Pa	Parameters				Research Findings	Ref.
		Laser Power	Scan Speed	Hatch Layer Spacing Thick	Hatch Layer Scan Spacing Thickness Strategy	Scan Strategy		
							• In the Z direction and nitrogen atmosphere, samples showed UTS of 385MPa, whereas, at XY direction and argon atmosphere, samples showed the lowest UTS of 338 MPa.  The samples fabricated in argon and nitrogen shows similar	
Mfusi et. al. (2019)	Mfusi et. al. (2019) SLM Solutions M280	150 W	1000 mm/s	50 µm 50 µm	50 µm	1	<ul> <li>defects &amp; microstructure.</li> <li>Anisotropy observed after heat treatment due to changed [103] build orientations.</li> </ul>	[103]
Cerri et. al. (2020)	Cerri et. al. (2020) SLM 500 SLM Solutions, Yb-YAG laser, 350 W Inert gas - Argon	350 W	1550 mm/s	17 μm 50 μm	50 µm	Horizontal sequential	Higher relative density was observed in XY print samples.  • The strain hardening is 0.19 to 0.25 & strength coefficient is [61] from 589 to 890 MPa.  Cabona countries is code to obtain 11TC subseque Datas according	[61]
						partern	canoni equation is used to obtain of a whereas retry equa- tion used to calculate YS.	

content of Si remains unchanged after the solubility of Si in the  $\alpha$ -Al matrix and the grain grows rapidly at higher temperature. During the succeeding aging, the Si precipitated evenly in the matrix and increased up to a certain extent. The heat treatment time is very important in T6 heat treatment. The too short time results in incomplete dissolve of the eutectic Si, whereas too long tome cause the serious coarsen of the grains, results in the deterioration of mechanical properties. The maximum strength of the materials can be achieved when the eutectic Si is fully dissolve and coarsen the grains [24]. Li et al. [28] observed the superfine microstructure in as-fabricated samples due to the higher cooling rate in printing that significantly improved the mechanical properties. Anwar et al. [75] exposed that the inert gas flow velocity and laser scan direction affects the microstructure. Xiong et. al. [83] studied the effect of melt pool boundary conditions on properties of SLMed AlSi10Mg alloy. The response of mechanical properties to melt pool boundaries was examined with the morphology and orientation of Al and Al-Si around the melt pool boundary. The microstructural analysis revealed that the melt pool mainly consist of columnar α-Al grains with the elongated cellular structure having length and width of around 1–3 μm and 0.5 μm respectively. The eutectic Si and Mg was also observed at the cell boundaries. Liu et. al. [79] designed and fabricated the box shaped structures with X shaped interior shelves to investigate the microstructural properties of SLMed AlSi10Mg alloy. The findings indicated that the build orientation affects the elongation direction of the columnar  $\alpha$  - Al in the melt pools and several columnar  $\alpha$ -Al enclosed by numerous fine Si particles were observed. These columnar  $\alpha$ -Al grains were elongated in the Z-direction. The higher cooling rate in printing process causes the elongation of  $\alpha$ -Al grains along the heat flow direction. The heterogeneous microstructure was observed in the crossing region of the X-shaped shelves. The  $\alpha$ -Al grains observed in the lower portion of X shelves are coarser and equiaxed as compared to the upper portion results in different hardness in these portions. Liu et. al. [27] studied the meander & remelting strategy to gain insight on variation of the microstructure & micro hardness with surface morphology, molten pool characteristics [122], relative density & phase identification. The results show that the laser remelting effectively enhances the surface roughness & relative density. The Ra value decreased to 9.94 µm from 13.34 µm i.e 25.49 % and the density increase from 2.60 g/cm3 to 2.66 g/cm3 also relative density increase from 97.2 % to 99.3 %. The finer microstructure with supersaturated  $\alpha$ - Al improves the hardness from 117.7 HV to 121.6 HV. Dong et. al. [65] elaborated the effect of build orientation on microstructure and tensile properties and mechanism of thermal heat transfer during SLM of AlSi10Mg samples. The microstructure size was influenced by the thermal behaviour in the melt pool. The difference in cooling rate at the core and surface region of melt pool affects the grain structure. In the surface region, the high cooling rate causes a fine cellular dendritic microstructure with a rich Si network in Al matrix, whereas the core of melt pool shows a coarser cellular dendritic microstructure. As the build angle increased from  $35.5^{\circ}$  to  $90^{\circ}$ , more than 12~%improvement in mechanical properties were observed.

### $2.4.\ Mechanical\ properties\ of\ additively\ manufactured\ AlSi10Mg\ alloy$

The mechanical properties of specimen were characterized through different test as per the ASTM standards. These properties are depends on the morphology and size of Si phase, the size of Al secondary dendrite spacing, the eutectic laminar spacing etc. and are mainly depend on the cooling rate. Also these properties vary significantly with the microstructure evolution during printing process and after post heat treatment. Kempen et. al. [18] investigated the tensile properties of AM produced AlSi10Mg parts and compared with the conventionally cast AlSi10Mg parts. The UTS

R.E. Gite and V.D. Wakchaure

Materials Today: Proceedings xxx (xxxx) xxx

**Table 4**Suggested ranges of SLM process parameters for additively manufactured AlSi10Mg alloy.

SLM Standard Parameters	Suggested Ranges	of SLM Process Parameters for	AlSi10Mg Alloy		
• Laser Type - Nd: YAG laser Wavelength 1060 - 1100 nm Laser Beam Spot Diameter - 70-100 μm Inert Gas - Argon	<b>Laser Power</b> 250 W – 350 W	Scan Speed * Continuous Wave laser 1200–2000 mm/s Pulsed Wave laser Point Distance 70–90 µm Exposure Time 40–60 µsec	<b>Scan Spacing</b> 80 μm – 120 μm	<b>Layer Thickness</b> 30 μm – 50 μm	<b>Scan Strategy</b> Stripes

<sup>\*</sup> For pulsed wave laser system, scan speed is not a direct editable parameter. It is calculated using the following formula.

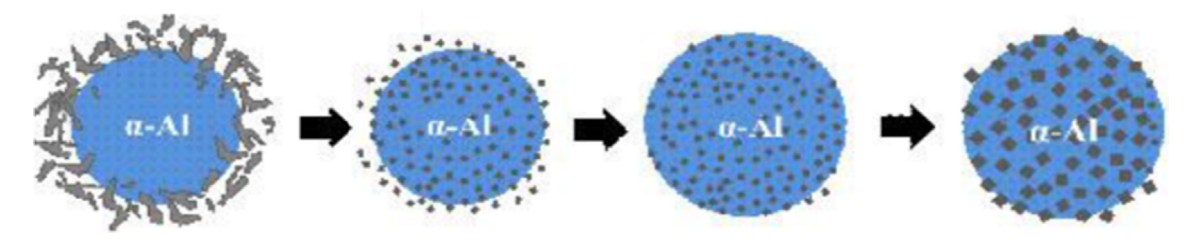


Fig. 2. Schematic diagram showing microstructure evolution mechanism [24].

of SLM parts was  $396 \pm 8$  MPa as compared to that of casted parts UTS of 300-317Mpa. The % elongation in SLM parts increases from 2.5 % to 5.5 %. The highest hardness achieved was 127 Hv in SLM & 86 Hv in casted parts. Mauduit et. al. [47] evaluated the material hardness and electrical conductivity, along with mechanical properties & microstructural changes of the AlSi10Mg alloy material & AlSi10Mg matrix composite. The UTS, yield strength & % elongation in the as-built state was 359 MPa, 308 MPa & 1.7 % & in heattreated specimens was 290 MPa, 262 MPa & 2.6 % respectively. The results show that a significant increase in the mechanical properties compared with casting. Wang et. al. [26] investigated the microstructure, structural performance and tensile fracture morphology at different orientations to analyse structural properties of AlSi10Mg alloy. The results observed were, ultimate tensile strength 315 MPa, yield strength 265 MPa, % elongation 5.36, impact energy 3.63 J and density 2.62 g/cm3 x-z direction. The SLM parts have higher mechanical properties as compare to the cast and forge material due to its superfine microstructure. The microstructure observed was fine equiaxed crystallites. Raus et. al. [77] investigated and compared the tensile properties of SLM AlSi10Mg specimens and conventionally die cast A360 alloy. The hardness and strength of SLM AlSi10Mg as built samples were improved by 42 % and 31 % respectively as compared to cast A360 alloy. The maximum density of 99.13 % was achieved with the optimized process parameters like laser power 350 W, scan velocity 1650 mm/s and hatch distance of 130 μm. Parveen et. al. [63] highlighted the effect of printing parameters on microstructure and tensile properties of AM AlSi10Mg alloy. The layer thickness of 30 µm and 60 µm, laser power of 170 W and 250 W with scan velocity of 500 mm/s and 700 mm/s were selected for investigation. It was observed that for both the layer thickness of 30 µm and 60 µm, the micro hardness didn't changes too much and observed 124 HV. The better mechanical properties of 30 µm layer thickness were observed as compared to 60 µm due to low porosity and superfine cellular dendritic microstructure. The UTS of 359 MPa and 446 MPa, YS of 232 MPa and 265 MPa and % elongation of 7.81 % and 9.63 % observed for 60 µm and 30 µm respectively. The horizontal built samples showed better mechanical properties as compared to vertically built samples.

So from the available research on comparative study of cast AlSi10Mg alloy [94,34,32,18,20], and SLM AlSi10Mg alloy, fine microstructure and higher mechanical properties were observed in SLM AlSi10Mg aluminium alloy and can be concluded that the AlSi10Mg is better candidate for selective laser melting.

#### 2.5. Heat treatment on additively manufactured AlSi10Mg alloy

Post heat treatments performed on additively manufactured AlSi10Mg Al alloys to improve the microstructure and mechanical properties. Usual treatments consists of heating and cooling to obtain recrystallization, different microstructures as well as get rid of impurities during manufacturing which results in an increase of strength and hardness of the alloy. Li et. al. [28] explored the influence of solution & aging heat treatments on the microstructures & tensile properties of SLMed AlSi10Mg alloy samples. The samples were heat treated at the various temperatures of 450 °C, 500 °C & 550 °C for 2 h, followed by quenching. The solubilities of Si in Al matrix for the samples treated at 450 °C, 500 °C, and 550 °C were 3.25, 2.75 and 2.13 % respectively. The as-fabricated specimen shows the highest tensile & yield strengths of 434.25  $\pm$  1 0.7 MPa & 322.17 ± 8.1 MPa, respectively but records the minimum ductility of 5.3  $\pm$  0.22 %. As the specimen was heat treated at 450  $^{\circ}$ C for 2 h, there was intensely decrease in both tensile & yield strengths (282.3  $\pm$  6.1 MPa & 196.58  $\pm$  3.6 MPa, respectively), with a huge increase in ductility of 13.4 ± 0.51 % was observed. Tradowsky et. al. [93] investigated the effect of post processing on microstructure and tensile properties of SLM AlSi10Mg. Fresh and recycled AlSi10Mg alloy [87] powder has been used to study the effect on mechanical properties. The samples prepared with recycled powder shows reduced mechanical properties as compared to the samples fabricated with new powder. The T6 and hot isostatic pressing post processing results in homogeneous microstructure with Si particles in Al matrix. The grain size observed was more significant in as build samples compared to HIP + T6 heat treated samples. The melt pool consists of dendrite cell network having cell size less than 1 µm. The equiaxed grains observed in cross section whereas the column like grains observed along build direction with width and diameter of about 5 µm. Takata et. al. [88] examined the variations in the microstructure & tensile properties of AlSi10Mg alloy produced by SLM. The as-built sample was held at 300 °C for 2 h (annealing) and at 530 °C for 6 h (SHT), followed by water quenching. The microstructure of the  $\alpha$ -Al matrix contains of elongated grains with a average width of 10 µm in the as-built sample. The hardness of the as-built sample significantly reduces from 132 HV to 88 HV after annealing and solution treatment, the hardness decreased to 60 HV. The as-built sample shows YS of 280 MPa in X/Y direction & tensile strength of 480 MPa. The elongation was around 8 %. In its counterpart in the Z direction, the YS were 230 MPa, whereas the UTS were at the same level. The tenR.E. Gite and V.D. Wakchaure

sile elongation was 5 %, which is minimum than in X/Y direction. Zhuo et.al [104] examined the influence on SLM AlSi10Mg by two kinds of heat treatment regimes, i.e. A1 (300 °C for 2 h and water quench) and A2 (535 °C for 1 h and water quench with 190 °C for 10 h and furnace quench). From the tensile test and nano indentation results, it was observed that the application of SLM with additional A1 heat treatment would result in a more reliable mechanical behaviour with engineering-required plasticity of no less than 10 % while keeping a relatively high strength of 273.18 MPa. Yu et. al. [90] deliberate the effect of two-stage T6 heat treatment on SLM fabricated AlSi10Mg alloy. The process included a SHT at 535 °C and ageing at 158 °C for 10 h. The effects of the T6 heat treatment on the density, hardness, and oxidation behaviour have been examined. Similar dinsity of 96 % in the asbuilt specimens and of 96.52 % in the heat treated samples shows that the T6 heat treatment has no importance to the density. The hardness decreased by about 20 % of heat treated specimens as compared to as-fabricated specimens. Wang et. al. [24] investigated the performance of SLM manufactured AlSi10Mg alloys after standard T6 heat treatment rather than conventional single stage heat treatment in the casting. The results show that the UTS of the heat treated specimens marginally decreased by 19.97 %, while the elongation exhibited a significant increase by up to 155 %. Similarly, the bending strength decreased by 6.1 %, while the fracture deflection increased by up to 122.9 % after heat treatment [105]. Fousova et.al [9] observed the changes in the SLM AlSi10Mg alloy after post process temperatures between 120 & 180 °C with a step of 20 °C and at each temperature, hardness evolution was measured. The maximum hardness observed at 160 °C & that was selected for investigation. At the systematically tested temperature of 160 °C, a small increase in yield strength but also a higher decrease in elongation was observed. Uzan et. al [106] investigated the tensile properties of SLMed AlSi10Mg specimens in the 25-400 °C temperature range. A annealing treatment at 300 °C for 2 h, carried out to improve the ductility of the material, resulted in an altering of Si-rich cellular boundaries. The result shows that the stress hardening takes place up to about 200 °C and above this temperature the mechanical behaviour is almost plastic. Creep experiments were conducted in the 225–300 °C temperature range under stress in the 117-147 MPa range. Rubben et. al. [2] studied the consequence of heat treatments on the microstructure and corrosion behaviour of AM AlSi10Mg specimens. Non heat treated, artificially aged and stress released specimens were studied. The aging at 170 °C for 6 h does not have a profound impact on microstructure. A annealing at 250 °C for 2 h causes the silicon network to initiate break-up into separate particles. By increasing the temperature of the stress release to 300 °C, the break-up is more complete and separate coarse silicon particles are formed. Girelli et. al [94] examined the impact of temperature & duration of heat and ageing treatment on microstructure, hardness & density of SLM AlSi10Mg alloy & gravity casting (GC). After ageing at 160 °C for 4 h, the hardness of 510 & 540 °C SHT samples increases up to 100 HBW, as compared to the samples treated at 480 °C, which was 20 % lower. The gravity cast samples, treated at 480 °C and aged at 160 °C for 4 h, the hardness of 80 HBW observed without considerable effects of heat treatment duration. Larrosa et. al. [57] analyzed the relation between the monotonic and cyclic behaviour of SLM produced AlSi10Mg samples with the presence of manufacturing defects such as pores, voids etc. and the significance of T6 and hot isotropic pressing treatment. The T6 treatment followed by hot isotropic pressing treatment reduces the porosity by 44 % for vertical build and 65 % for the horizontal build. No improvement observed in mechanical properties. However the higher yield strength was observed due to the cell like regions of about 350 nm diameter of Al grains. These regions were sur-

rounded by 10 nm thick regions of Si. Maamoun et. al. [95] studied the consequence of post processing on fresh and recycled AlSi10Mg alloy powder. Three types of heat treatments, annealing [107], solution heat treatment and T6 treatment was applied on asfabricated samples to understand the effect on microstructure. The fibrous Si network was decomposed and fine Si particles observed around the Al grains after annealing, whereas for the T6 and solution heat treated samples, large Si particles inside the Al matrix with Mg2Si precipitates was observed. The generated residual stresses after machining were relief after annealing. The T6 and solution heat treatment leads to residual stresses on the surface of part. Rautio et. al. [108] elaborated the effect of surface heat treatment on the SLM printed AlSi10Mg specimen with disk laser equipment having a wavelength of 1030 nm with robotized laser heat treatment. Surface treatments were carried out by experimenting with the laser parameters that are Laser power, speed and the amount of overlap between the laser paths. The effect of repeating the same treatment on the surface has experimented. Jiang et. al. [102] investigated a method for simulating the heat treatment of AlSi10Mg, where the real-time changes of microstructure, grain size & residual stress in the heat treatment were analysed by building 3D models and software simulation to save time and cost. The results show minimum residual stresses when the heating temperature was 350 °C as compare to 550 °C. The strength decreases by 40 % and the plasticity increases by 2.8 times. The plasticity of SLM AlSi10Mg alloy specimens was significant improved after heat treatment. Zhang et. al. [60] explored the effect of overlap on defects, microstructure and tensile properties of SLM samples manufactured by single laser and multi laser beam. In SLM the melt pool appears with three different zones: at centre, fine cellular dendrite surrounded by course cellular dendrite and the heat affected zone at outside boundary of melt pool. The Si particles are separated in the HAZ due to the local thermal effect. The results show that the samples produced by single laser and multi laser beam didn't affect the microstructure and mechanical properties. The average micro hardness was 137  $\pm$  2 HV and 136  $\pm$  2 HV for isolated and overlap samples. The ultimate tensile strength was  $395 \pm 1$  for Isolated and  $389 \pm 4$  for Overlap samples. The yield strength observed was 276 ± 2 for Isolated and 273 ± 6 for Overlap samples. The % elongation increases to 5  $\pm$  0.5 for Isolated and  $4.4 \pm 0.4$  for Overlap samples.

Table 5 summarizes the heat treatment applied and mechanical properties of AM AlSi10Mg alloy. From the available literature it is observed that two types of heat treatments, conventional (elevated temperature) and stress relieving (Annealing) are applied on the SLM samples. The conventional heat treatment operated at elevated temperature ranging from 450 °C to 550 °C, followed by ageing, whereas as stress relieving heat treatment operated at 300 °C for 2 h. The available researches on these heat treatments and effect on mechanical properties of SLM AlSi10Mg alloy has been summarized here.

#### 3. Directions for future research

Although several studies have been carried out and high-lighted the various aspects from powder characterization to post-processing of SLM AlSi10Mg parts, there are still some of the grey areas that need to be addressed and further study required in this regard. The gaps identified from the literature are listed below.

 From the literature available it is observed that most of the researchers focused on microstructure and mechanical properties of SLM AlSi10Mg alloy with limited selective process parameters like scan speed, hatch spacing and laser power. It

Ref.

[92]

[123]

[101]

[60]

**Heat Treated** 

100 ± 1 HV

51 HV

103 ± 3 HV

Author

(Year)

Aboulkhair

et. al. (2016)

Rosenthal

Qi et. al. (2018)

et. al.

(2016)

Zhang et. al.

Materials Today: Proceedings xxx (xxxx) xxx

(continued on next page)

**Table 5**Summary of heat treatment and mechanical properties of SLM AlSi10Mg alloy.

**Mechanical Properties** 

481 ± 2 (Isolated),

As-built

333 ± 15

Ultimate Tensile Strength (MPa)

**Heat Treated** 

282 ± 5 (XY),

395 ± 1 (Isolated),

 $288 \pm 5 (Z)$ 

292 ± 4

**Heat Treatment** 

520 °C + Artificial

ageing 160 °C, 6 h

550 °C, 2 h, furnace

Annealing, 300 °C,

300 °C, 2 h

cooling

SHT

	2 h, furnace coolin	481 ± 2 (Isolated), g 471 ± 7 (Overlap)	389 ± 4 (Ov	389 ± 4 (Overlap) 316 ± 7 (Overlap)			3.0 ± 0.2 (Overla)		(Isolated), 136 ± (Overlap)	2 (Isolated), 102 ± 3 (Overlap)	[60]
Wang et. al. (2017)	-	364 (XY) & 315 (Z)	-	303 (XY) & 265 (Z)	-	(	5.7 (XY) & 5.36 (	Z) –	-	-	[26]
Raus et. al. (2017)	-	412 ± 2	<b>-</b> ,	242 ± 5	-	(	5.34 ± 0.3	-	139 HV, 149 HV	-	[77]
Xiong et. al. (2018)	-	360 (XY), 363 (Z)	-	220 (XY), 190 (Z)	-	7	7.1 (XY), 4.3 (Z)	-	-	-	[83]
Amani et. al. (2018)	-	267 ± 10 (XY), 273 ± 10 (Z)	-	169 ± 4 (XY), 169 ± 5 (Z)	-		9.1 ± 1.9 (XY), 3.2 ± 1.2 (Z)	-	-	-	[58]
, ,	-	391 ± 6 (XY), 396 ± 8 (Z)	-	_	-	į	5.55 ± 0.4 (XY), 3.47 ± 0.6 (Z)	-	-	-	[18]
	Annealing, 300 °C, 2 h	300	113	208	101	1	18	29	-	-	[72]
Author (Year)	Heat Treatm	ent	Mechanica	l Properties							Ref.
			Ultimate T	ensile Strength (MPa)	Yield Stre	ngth (MPa)	Elongation	(%)	Hardness		
			As-built	Heat Treated	As-built	Heat Treated	As-built	Heat Treated	As-built	Heat Treated	
Takata et. al. (2017)	SHT, 530 °C,	6h, water quenching	475 (XY), 476 (Z)	SHT - 269 (XY), 245 (Z)	279 (XY), 220 (Z0	SHT 153 (XY), 139 (Z)	7.5 (XY), 5.5 (Z)	SHT 18.3(XY), 18.1 (Z)	132 HV	SHT - 60 HV, Aging - 75 HV	[88]
	Annealing, 3 quenching	00°C, 2h, water		Annealing 285 (XY), 290 (Z)		Annealing 180(XY), 175 (Z)	;	Annealing 18.6(XY), 14.2 (Z)		Annealing — 88 HV	
Mauduit et. al. (2015)	540 °C, 1h + A quenching	Artificial Aging 160 °C, 5h	Room Temp – 456 (XY)	Room Temp – 312 (XY)	Room Temp – 368 (XY)	-	Room Temp – 3 (XY)	Room Temp – 3.2 (XY)	95 HBW	140 HBW (After artificial ageing)	[47]
			180 °C − 348 (XY)	180 °C – 251 (XY)	180 °C – 253 (XY)	-	180 °C − 3.3 (XY)	-			
			Room Temp – 359.5 (Z)	Room Temp – 290 (Z)	Room Temp – 306.5 (Z)	Room Temp – 262 (Z)	Room Temp – 1.7 (Z)	Room Temp – 2.5 (Z)			
			180 °C – 285 (Z)	-	180 °C – 213 (Z)	180 °C – 198 (Z)	1.7 (Z) 180 °C − 3.5 (Z)	180 °C - 1.6 (Z)			
Li et. al. (2016)		C & 550 °C, 2h,water 0 % samples (artificial °C for 12h)	434 ± 10.7	282 ± 6.1 (SHT 450 °C for2h)	322 ± 8.1	196 ± 3.6 (SHT 450 °C for2h)		13.4 ± 0.51 (SHT 450 °C for2h)	132.5 ± 5.3	96.65 ± 3.6 (SHT 450 °C for2h), 78.15 ± 2.8 (SHT 450 °C for 2h + 180°C for 12h)	[28]
				213 ± 4.6 (SHT 500 °C 2h),197 ± 3.5 (SHT 500 °C		126 ± 2.1 (SHT		23.5 ± 0.81 (SHT 500 °C 21 23.8 ± 0.87(SHT 500 °C 2h	,,	87.85 ± 3.1 (SHT 500 °C 2h), 60.55 ± 1.7 (SHT	

Yield Strength (MPa)

As-built

268 ± 2

200

**Heat Treated** 

182 ± 5 (XY),

184 ± 5 (Z)

100

239 ± 2

Elongation (%)

As-built

 $1.4 \pm 0.3$ 

6

 $314 \pm 6$  (Isolated),  $276 \pm 2$  (Isolated)  $3.3 \pm 0.2$  (Isolated),  $5 \pm 0.5$  (Isolated),

Hardness

As-built

123 HV

137 ± 2 HV

125 ± 1 HV

**Heat Treated** 

 $7.6 \pm 0.05$  (XY),

 $7.2 \pm 0.05 (Z)$ 

 $3.9 \pm 0.5$ 

Table 5 (continued)

Author (Year	r) Heat Treatment	Mechanical Pr	operties											Ref
		Ultimate Tensi	le Strengt	h (MPa)	Yield St	trength (MP	a) Elo	ngation (%)		Hardness	3			_
		As-built H	eat Treate	đ	As-buil	t Heat Treated		built Hea	t Treated	As-built	Heat Tr	eated		
		10 18		12h) HT 550°C 2h), HT 550°C 2h+		500 °C 90 ± 1.6 (SHT 550 °C	<b>5</b>	23.7 2h),	°C 12h), 7 ± 0.84 (SHT 550 °C 19.5 ± 0.6 (SHT 550 °C + 180°C for 12h	2	63.55 ±	1.9 (SI ± 1.4	80°C 12h) HT 550°C (SHT 550°C h	
Author	Heat Treatment	Mechanical	Properties											Ref
(Year)		Ultimate Ter	ısile Stren	gth (MPa)		Yield Stren	gth (MPa)	)	Elongation (%)		1	Hardne	ess	
		As-built		Heat Treated	1	As-built	Heat Tre	eated	As-built	Heat Treate		As- puilt	Heat Treated	
Ch et. al. (2017)	-	364.9±1.6 (A 338.51±2.449 XY),	(Argon -	-		-	-		15.58±1.9 (Argon - Z), 18.37±1.357 (Argon XY),	-	-	_	-	[34
		386.93 ± 3.93 (Nitrogen Z), 358.70 ± 2.3 XY), 300–317 (As	(Nitrogen	-		_	-		22.0±2.11 (Nitrogen Z), 19.40±2.1 (Nitrogen XY), 2.5–3.5 (As cast)	-	-	-	-	
Tradowsky	SHT (T6) 520°C, 5h, water quenching + Aging	370 370	Cast)	310 (T6)		270	270 (T6)		5	4 (T6)	-	-	-	[93
et. al. (2016)	HT – 160°C, 12h, air cooling HIP 530°C, 2h, heating & cooling rate – 5° C/ min			140 (HIP)			120 (HIP	)		23 (HIP)				
Zhuo et. al. (2018)	SHT-535°C, 1h, water quenching + Ageing 192°C, 10h, furnace quenching Annealing, 300°C, 2h, water quenching	446.28		SHT 273.18 Annealing 21	2.65	270.01	SHT 169.		8.09	SHT 15.27 Annealing 1	(	2.098 GPa	SHT 1.610 GPa Annealing	
													1.456 GPa	
Girelli et. al. (2019)	480°C, 510°C, 540°C, 1h, 3h, 6h, 9h, water quenching 65°C, heating rate 3°C/ min + Ageing 160°C, 5h, Air cooling	452 ± 1 (XY) (Z)	, 482 ± 1	332 ± 1 (XY), 299 ± 24 (Z) @ 1h – 180 °C 2	9540 °C	264 ± 4 (XY), 247 ± 1 (Z)	277 ± 1 ( 248 ± 14 @540 °C 2h		8.6 ± 1 (XY), 6.5 ± 0.3 (Z)	5.6 ± 0.2 (X 5.1 ± 1.1 (Z) 1h – 180 °C	, @540 °C l	125 HBW	108 HBW	[94
Author	Heat Treatment		Mechanie	cal Properties										Ref.
(Year)			Ultimate	Tensile Streng	th (MPa)	Yield Str	ength (MF	Pa)	Elongation (%)		Hardness			
			As-built		leat Treated	As-built		Heat Treated	As-built	Heat Treated	As-built		leat reated	
Fousova et. al. (2018)	SHT (T6), 530 °C, 6h, water quenching + Ageing cooling	g 160°C, 5h, Air	377 ± 13	2	SHT 284 ± 12, 342 ± 8 160 °C)	255 ± 13		SHT 210 ± 11, 268 ± 21 (160 °C)	2.2 ± 0.2	SHT 9.9 ± 0.4, 0.9 ± 0.2 (160 °C)		Н	40.7 ± 1.3 IV1 (at 60 °C)	[9]
	Annealing, 300 °C, 2h			Ä	Annealing 256 ± 10	;		Annealing	g	Annealing 9.9 ± 0.4		-		
Wang et. al. (2018)	SHT, 535 °C, 2h, heating rate – 10 °C/ min sa quenching + Ageing 158 °C, 10h, Room temp, 10 °C/ min		358 (XY),		278 (XY), 267.3 (Z)	-		160(XY), 174 (Z)	3.64 (Z)	9.28 (Z)	103.2 HB (XY), 102.2 HB (Z)	()	8.7 HB XY), 83.5 IB (Z)	[24]
Iturrioz et. al. (2018)	450 & 550 °C, 2h, water quenching 300 °C, 2h		382	2	807 ± 8 220			248 ± 2	2.3	9 ± 3% 17%	127 ± 5 HV	1	01 ± 4 HV	[113
Beretta et. al. (2020)	-			(0°), 375- 387-409	-		(0°), 203– 207–209		4.3-5 (0°), 4.5- 6.7 (45°), 4.7-6.1 (90°)	_	-	-		[62]

Table 5 (continued)

	Heat Treatment		Mechanica	l Properties	6								Ref.
(Year)			Ultimate T	ensile Stren	gth (MPa)	Yield St	ength (MPa	a)	Elongation (%)		Hardness		
			As-built		Heat Treated	As-built		Heat Treated	As-built	Heat Treated	As-built	Heat Treated	
Parveen et al. (2021)	-		359 (60μm (30μm)	1), 446	-	232 (60 <sub>µ</sub> (30 <sub>µ</sub> m)	ım), 265	-	7.81 (60µm), 9.63 (30µm)	-	-	-	[63]
(2021) Aboulkhair - et. al. (2020)	-		320		-	175		-	3	-	109.7 ± 0.9 HV (XY)	99.07 ± 2 HV (Z)	[42]
Dong et. al. (2019)	-		360.7 ± 5.8	3	-	176.3 ±	2.4	-	2.92 ± 0.09	-	-	-	[65]
	530°C, 8h + Artificial Aging 170°C for 18	h	399		_	241		-	3.15	-	_	-	[65]
Author (Year)	Heat Treatment		Mechanical Proper										Ref.
			Ultimate Tensile St (MPa)	rength	Yield Stre (MPa)	ength	Elongatio	n (%)	Hardness				
			As-built	Heat Treated	As- built	Heat Treated	As-built	Heat Treated	As-built		Heat Treate	d	
Martin et.al. (2017)	-		315	-	209	-	7.3	-	-		-		[23]
Pei et. al. (2017)	-		360 at scan speed 1000mm/s	-	-	-	-	-	2.25±0.1 GPa to 2.71±0 bottom surface, Z)	0.1 Gpa (Top to	O –		[78]
			336 at scan speed 800 mm/s	-	-	-	-	-	-	0.1.6	_		
			305 at scan speed 1400mm/s	-	_	_	_	_	2.31±0.1 GPa to 2.82± (Centre to edge, XY)	0.1 Gpa	_		
Maskery et. al (2016)	520 °C, 1h, water quench + Artificial Ag for 6h	ing 160 °C	330 ± 10	292 ± 4	_	-	-	-	=		-		[49]
Sajadi et. al. (2021)	SHT 300,400,500 °C, + Ageing 140, 160		347 ± 5	305 ± 3	187 ± 3	240 ± 3	4.5 ± 0.3	6 ± 0.3	-		_		[97]
Mertens et. al. (2015)	ageing at 150 °C, 170 °C		-	-	=	-	=	-	127 ± 3 Hv		-		[98]
Alghamdi et. al. (2019)	520 °C, 1h, water quenching, Artificial 170 °C, 4h.			-	-	-	-	-	112.7 ± 2.4 HV (XY), 1 (Z)	115.7 ± 3.5 HV	94.4 ± 2.84, 97.3 ± 2.8 H		[114]
Author (Year)	Heat Treatment		al Properties						400				Ref.
		Ultimate	Tensile Strength (MP	'a)		(MPa)	trength	Elongatio	on (%)		Hardness		
		As-built			Heat Treated	As- I built	Heat Treated	As-built		Heat Treated	As-built	Heat Treated	
	SHT, 520 °C, 5h, water quenching + Ageing 160 °C, 12h, Air cooling	370			275	250	230	1		2	-	-	[57]
, ,	HIP, 530 °C, 2h, heating rate – 5 °C/ min, cooling rate 5 °C/min				140		120			7		-	
Maamoun	SHT, 530 °C, 1h, 530 °C, 5h water quenching + Ageing 160 °C, 11h	-			-	_	-	-		-	120 ± 2 HV	115 HV	[95]
Jiang et. al. (2019)	250 °C to 550 °C, 2h water quenching + Tempering 160 °C, 2h, Air cool 5h	387.4			168.8	-	-	3.22		9.15	-	-	[102
Ch et. al. (2019)	-		Nitrogen XY), 385 ± 5 Argon, XY), 366 ± 4 (A		), –	-	-		gen XY), 4.5 (Nitrogen 2 n, XY), 4.4 (Argon, Z)	Z), –		-	[34]

(communa)	aca)									
Author	Heat Treatment	Mechanical Properties								Ref.
(Year)		Ultimate Tensile Strength (MPa)		Yield Str (MPa)	ength	Yield Strength Elongation (%) (MPa)		Hardness		
		As-built	Heat Treated	As- built	Heat As- Heat As-built Treated built Treated	As-built	Heat Treated	As-built Heat Treated	Heat Treated	
Liu et. al. (2017)	1	ı	I	ı	I	ı	I	148 ± 7 HV & -	1	[26]
Rosenthal et. al.	Stress relief at 250 °C – 2h,	473 ± 1	286 ± 2	263 ± 5	286 ± 2 263 ± 5 183 ± 5 7.8 ± 0.1	7.8 ± 0.1	18.7 ± 1.2		110 ± 5 HV	[109]
(2018)	HIP 500 °C – 2h		184 ± 1		115 ± 5		$38.8 \pm 1.0$		60 ± 5 HV	
									^ 1	

is necessary to consider other important parameters like layer thickness, pulse duration, scan pattern etc. which contributes to SLM product getting distinct microstructure and mechanical properties.

- In the post-processing, two types heat treatments applied on AM samples, one is solution heat treatment with the temperature ranges between 450 and 550 °C followed by ageing treatment between 150 and 180 °C and other is annealing at 300 °C for 2 h. It would be interesting to know the effect of ageing temperature after annealing on the post-heat treatment properties of AlSi10Mg.
- In the post-processing, some of the authors studied & exposed the effect of ageing temperature and time, while other authors disclosed the influence of the heating temperature only. This need to extend further and the combined effect need to be studied.
- Standard T6 heat treatment, designed for conventionally manufactured parts, was implemented on AM AlSi10Mg alloy. It leads to softening of the material and affects the microstructure and mechanical properties. So, the specific heat treatment process for AM components needs to be designed.
- A SHT, quenching and ageing heat treatment are often executed on additively manufactured AlSi10Mg parts to dissolve the anisotropy developed due to the layer over layer building. The material shows different behaviour in both directions (X-Y & Z). This anisotropy further affects mechanical properties. The anisotropy needs to be reduced by selecting the custom-tailored heat treatment with optimized parameters.
- Very little attention is given on the optimization of the significant heat treatment parameters like heating temperature, heating rate, cooling rate, cooling temperature etc. An optimization model considering all these parameters has not yet been developed for understanding the influence of heat treatment on mechanical properties of AlSi10Mg alloy.
- The energy density is one of the important parameters in SLM & there is no direct relationship between the energy density & part quality. It is clear that only energy density is not able to completely represent the SLM process.
- The literature is silent on the behaviour of 3D printed AlSi10Mg alloy material subjected to the cryogenic treatment. The cryogenic treatment combined with traditional heat treatment can improve the microstructure, density, dimensional stability and reduces the residual stresses generated in SLM. Such information is essential for the improvement in mechanical properties and removal of residual stresses induced in the specimen.

These gaps need be addressed to improve the mechanical properties and can be achieved by the employment of the optimization model for the SLM process.

#### 4. Conclusion

After studying the process parameters, mechanical properties and post processing on additively manufactured AlSi10Mg alloy following conclusions were made.

- The important printing parameters like laser power, scan velocity, scan spacing and layer thickness plays an important role in the SLM process as they directly affect the microstructure and mechanical properties of AM product. So to get better result, it is necessary to select the precise process parameters using optimization techniques.
- The microstructure is affected by the cooling rate, melt pool formation, thermal gradient, laser parameters & alloy composition.
   The rapid solidification, shallower melt pool and thermal gradi-

ent during SLM are responsible for the formation of fine microstructure. This fine microstructure is the reason for high mechanical properties

- The ultimate tensile strength and yield strength of SLM produced as-fabricated specimens were observed higher due to the superfine microstructure caused by rapid cooling rate in SLM. But this higher cooling rate responsible for the defects such as porosity, cracks, residual stresses and brittleness in the part results in poor functional properties of AM parts.
- The heat treatment method can effectively eliminate the residual stress. The output quality after heat treatment is influenced by several factors, such as size, number and morphology of the Si phases, initial hardening rate and recovery rate.
- For the heat treated samples a remarkable increase in % elongation is observed. Not too much difference in % elongation observed for annealing and solution heat treated samples. Similar results were observed for hardness also. Slight improvement in hardness observed after artificial ageing.
- The discussions on SLM process parameters, heat treatment and mechanical properties are presented here and need to be perceived further.

#### Data availability

Data will be made available on request.

#### **Declaration of Competing Interest**

The authors declare that they have no known competing financial interests or personal relationships that could have appeared to influence the work reported in this paper.

#### Acknowledgements

The authors are extremely thankful to Savitribai Phule Pune University, Pune, Amison Engineering, Pune and Research Centre, Amrutvahini College of Engineering, Sangamner, Dist. Ahmednagar (M.S.) India, for the technical and resource support to conduct this research work.

#### References

- [1] I. Maskery, N.T. Aboulkhair, M.R. Corfield, C. Tuck, A.T. Clare, R.K. Leach, R.D. Wildman, I.A. Ashcroft, R.J.M. Hague, Quantification and characterisation of porosity in selectively laser melted Al-Si10-Mg using X-ray computed tomography, Mater. Charact. 111 (2016) 193–204, https://doi.org/10.1016/imatchar.2015.12.001.
- [2] T. Rubben, R.I. Revilla, I. De Graeve, Influence of heat treatments on the corrosion mechanism of additive manufactured AlSi10Mg, Corros. Sci. 147 (2019) 406–415, https://doi.org/10.1016/j.corsci.2018.11.038.
- [3] N.T. Aboulkhair, M. Simonelli, L. Parry, I. Ashcroft, C. Tuck, R. Hague, 3D printing of Aluminium alloys: additive Manufacturing of Aluminium alloys using selective laser melting, Prog. Mater. Sci. vol. 106 (July 2019), https://doi.org/10.1016/j.pmatsci.2019.100578 100578.
- [4] J. Mäkikangas, T. Rautio, A. Mustakangas, K. Mäntyjärvi, Laser welding of AlSi10Mg aluminium-based alloy produced by Selective Laser Melting (SLM), Procedia Manuf. 36 (2019) 88–94, https://doi.org/10.1016/j. promfg.2019.08.013.
- [5] D. Brough, H. Jouhara, The aluminium industry: A review on state-of-the-art technologies, environmental impacts and possibilities for waste heat recovery, Int. J. Thermofluids 1–2 (2020), https://doi.org/10.1016/j. ijft.2019.100007 100007.
- [6] N. Li, S. Huang, G. Zhang, R. Qin, W. Liu, H. Xiong, G. Shi, J. Blackburn, Progress in additive manufacturing on new materials: a review, J. Mater. Sci. Technol. 35 (2) (2019) 242–269, https://doi.org/10.1016/j.jmst.2018.09.002.
- [7] T.H. Park, M.S. Baek, Y. Sohn, K.A. Lee, Effect of post-heat treatment on the wear properties of AlSi10Mg alloy manufactured by selective laser melting, Arch. Metall. Mater. 65 (3) (2020) 1073–1080, https://doi.org/10.24425/ amm.2020.133220.
- [8] J. Zhang, B. Song, Q. Wei, D. Bourell, Y. Shi, A review of selective laser melting of aluminum alloys: processing, microstructure, property and developing trends, J. Mater. Sci. Technol. 35 (2) (2019) 270–284, https://doi.org/10.1016/ i.imst.2018.09.004.

- [9] M. Fousová, D. Dvorský, A. Michalcová, D. Vojtěch, Changes in the microstructure and mechanical properties of additively manufactured AlSi10Mg alloy after exposure to elevated temperatures, Mater. Charact. 137 (January 2018) 119–126, https://doi.org/10.1016/j.matchar.2018.01.028.
- [10] P. Anant Pidge, H. Kumar, Additive manufacturing: A review on 3 D printing of metals and study of residual stress, buckling load capacity of strut members, Mater. Today Proc. vol. 21 (2020) 1689–1694, https://doi.org/ 10.1016/j.matpr.2019.12.012.
- [11] J. Wu, L. Wang, X. An, Numerical analysis of residual stress evolution of AlSi10Mg manufactured by selective laser melting, Optik (Stuttg) 137 (2017) 65–78, https://doi.org/10.1016/j.ijleo.2017.02.060.
- [12] T. DebRoy, H.L. Wei, J.S. Zuback, T. Mukherjee, J.W. Elmer, J.O. Milewski, A.M. Beese, A. Wilson-Heid, A. De, W. Zhang, Additive manufacturing of metallic components process, structure and properties, Prog. Mater. Sci. 92 (2018) 112–224, https://doi.org/10.1016/j.pmatsci.2017.10.001.
- [13] A. Salmi, E. Atzeni, History of residual stresses during the production phases of AlSi10Mg parts processed by powder bed additive manufacturing technology, Virtual Phys. Prototyp. 12 (2) (2017) 153–160, https://doi.org/ 10.1080/17452759.2017.1310439.
- [14] S. Kleiner, J. Zürcher, O. Bauer, P. Margraf, Heat treatment response of selectively laser melted AlSi10Mg, HTM - J. Heat Treat. Mater. 75 (5) (2020) 327-341, https://doi.org/10.3139/105.110418.
- [15] T. Chen, L. Wang, S. Tan, Effects of vacuum annealing treatment on microstructures and residual stress of AlSi10Mg parts produced by selective laser melting process, Mod. Phys. Lett. B 30 (19) (2016) 1–13, https://doi.org/ 10.1142/S0217984916502559.
- [16] L. Zhuo, Z. Wang, H. Zhang, E. Yin, Y. Wang, T. Xu, C. Li, Effect of post-process heat treatment on microstructure and properties of selective laser melted AlSi10Mg alloy, Mater. Lett. 234 (2019) 196–200, https://doi.org/10.1016/ j.matlet.2018.09.109.
- [17] K. Kempen, L. Thijs, E. Yasa, M. Badrossamay, W. Verheecke, and J. P. Kruth, "Process optimization and microstructural analysis for selective laser melting of AlSi10Mg," 22nd Annu. Int. Solid Free. Fabr. Symp. - An Addit. Manuf. Conf. SFF 2011, no. May 2014, pp. 484–495, 2011.
- [18] K. Kempen, L. Thijs, J. Van Humbeeck, J.P. Kruth, Mechanical properties of AlSi10Mg produced by selective laser melting, Phys. Procedia 39 (2012) 439– 446, https://doi.org/10.1016/j.phpro.2012.10.059.
- [19] P. Ponnusamy, R.A.R. Rashid, S.H. Masood, D. Ruan, S. Palanisamy, Mechanical properties of slm-printed aluminium alloys: a review, Materials (Basel) 13 (19) (2020) 1–51, https://doi.org/10.3390/ma13194301.
- [20] K. Zyguła, B. Nosek, H. Pasiowiec, and N. Szysiak, "Mechanical properties and microstructure of AlSi10Mg alloy obtained by casting and SLM technique," vol. 104, no. July, pp. 462–472, 2018
- [21] S. Hegde, K.N. Prabhu, Modification of eutectic silicon in Al-Si alloys, J. Mater. Sci. 43 (9) (2008) 3009–3027, https://doi.org/10.1007/s10853-008-2505-5.
- [22] E. Louvis, P. Fox, C.J. Sutcliffe, Selective laser melting of aluminium components, J. Mater. Process. Technol. 211 (2) (2011) 275–284, https://doi.org/10.1016/j.jmatprotec.2010.09.019.
- [23] J.H. Martin, B.D. Yahata, J.M. Hundley, J.A. Mayer, T.A. Schaedler, T.M. Pollock, 3D printing of high-strength aluminium alloys, Nature 549 (7672) (2017) 365–369, https://doi.org/10.1038/nature23894.
- [24] L.F. Wang, J. Sun, X.L. Yu, Y. Shi, X.G. Zhu, L.Y. Cheng, H.H. Liang, B. Yan, L.J. Guo, Enhancement in mechanical properties of selectively laser-melted AlSi10Mg aluminum alloys by T6-like heat treatment, Mater. Sci. Eng. A 734 (2018) 299–310.
- [25] K. Bartkowiak, S. Ullrich, T. Frick, M. Schmidt, New developments of laser processing aluminium alloys via additive manufacturing technique, Phys. Procedia vol. 12 (PART 1) (2011) 393–401, https://doi.org/10.1016/j. phpro.2011.03.050.
- [26] L. Wang, X. Jiang, M. Guo, X. Zhu, B. Yan, Characterisation of structural properties for AlSi10Mg alloys fabricated by selective laser melting, Mater. Sci. Technol. (United Kingdom) 33 (18) (2017) 2274–2282, https://doi.org/ 10.1080/02670836.2017.1398513.
- [27] B. Liu, B. Q. Li, and Z. Li, "Selective laser remelting of an additive layer manufacturing process on AlSi10Mg," *Results Phys.*, vol. 12, no. November 2018, pp. 982–988, 2019, doi: 10.1016/j.rinp.2018.12.018.
- [28] W. Li, S. Li, J. Liu, A. Zhang, Y. Zhou, Q. Wei, C. Yan, Y. Shi, Effect of heat treatment on AlSi10Mg alloy fabricated by selective laser melting: Microstructure evolution, mechanical properties and fracture mechanism, Mater. Sci. Eng. A 663 (2016) 116–125, https://doi.org/10.1016/j. msea.2016.03.088.
- [29] E. Brandl, U. Heckenberger, V. Holzinger, D. Buchbinder, Additive manufactured AlSi10Mg samples using Selective Laser Melting (SLM): microstructure, high cycle fatigue, and fracture behavior, Mater. Des. 34 (2012) 159–169, https://doi.org/10.1016/j.matdes.2011.07.067.
- [30] E. Zaretsky, A. Stern, and N. Frage, "Dynamic response of AlSi10Mg alloy fabricated by selective laser melting," *Mater. Sci. Eng. A*, vol. 688, no. December 2016, pp. 364–370, 2017, doi: 10.1016/j.msea.2017.02.004.
- [31] L. Thijs, K. Kempen, J.P. Kruth, J. Van Humbeeck, Fine-structured aluminium products with controllable texture by selective laser melting of pre-alloyed AlSi10Mg powder, Acta Mater. 61 (5) (2013) 1809–1819, https://doi.org/10.1016/j.actamat.2012.11.052.
- [32] P. Tonolini, L. Montesano, M. Tocci, A. Pola, M. Gelfi, Wear behavior of AlSi10Mg alloy produced by laser-based powder bed fusion and gravity casting, Adv. Eng. Mater. 23 (10) (2021) 2100147.

Materials Today: Proceedings xxx (xxxx) xxx

R.E. Gite and V.D. Wakchaure

- [33] X.J. Wang, L.C. Zhang, M.H. Fang, T.B. Sercombe, The effect of atmosphere on the structure and properties of a selective laser melted Al-12Si alloy, Mater. Sci. Eng. A 597 (2014) 370–375, https://doi.org/10.1016/j.msea.2014.01.012.
- [34] C.H.S. Rakesh, N. Priyanka, R. Jayaganthan, N.J. Vasa, Effect of build atmosphere on the mechanical properties of AlSi10Mg produced by selective laser melting, Mater. Today Proc. 5 (9) (2018) 17231–17238, https://doi.org/10.1016/j.matpr.2018.04.133.
- [35] B. Ferrar, L. Mullen, E. Jones, R. Stamp, C.J. Sutcliffe, Journal of materials processing technology gas flow effects on selective laser melting (SLM) manufacturing performance, J. Mater. Process. Tech. 212 (2) (2012) 355–364, https://doi.org/10.1016/j.jmatprotec.2011.09.020.
- [36] A. Masmoudi, R. Bolot, C. Coddet, Investigation of the laser-powder-atmosphere interaction zone during the selective laser melting process, J. Mater. Process. Technol. 225 (2015) 122–132, https://doi.org/10.1016/j.imatprotec.2015.05.008.
- [37] T. Yang, T. Liu, W. Liao, E. MacDonald, H. Wei, X. Chen, L. Jiang, The influence of process parameters on vertical surface roughness of the AlSi10Mg parts fabricated by selective laser melting, J. Mater. Process. Technol. 266 (2019) 26–36, https://doi.org/10.1016/j.jmatprotec.2018.10.015.
- [38] C.A. Biffi, J. Fiocchi, P. Bassani, A. Tuissi, Continuous wave vs pulsed wave laser emission in selective laser melting of AlSi10Mg parts with industrial optimized process parameters: Microstructure and mechanical behaviour, Addit. Manuf. 24 (October 2018) 639–646, https://doi.org/10.1016/j. addma.2018.10.021.
- [39] X. Ding, L. Wang, S. Wang, Comparison study of numerical analysis for heat transfer and fluid flow under two different laser scan pattern during selective laser melting, Optik (Stuttg) 127 (22) (2016) 10898–10907, https://doi.org/ 10.1016/j.ijleo.2016.08.123.
- [40] B. Qian, Y.S. Shi, Q.S. Wei, H.B. Wang, The helix scan strategy applied to the selective laser melting, Int. J. Adv. Manuf. Technol. 63 (5–8) (2012) 631–640, https://doi.org/10.1007/s00170-012-3922-9.
- [41] L. Hitzler, C. Janousch, J. Schanz, M. Merkel, B. Heine, F. Mack, W. Hall, A. Öchsner, Direction and location dependency of selective laser melted AlSi10Mg specimens, J. Mater. Process. Technol. 243 (2017) 48–61, https://doi.org/10.1016/ji.jmatprotec.2016.11.029.
- [42] N. T. Aboulkhair, A. Stephens, I. Maskery, C. Tuck, I. Ashcroft, and N. M. Everitt, "Mechanical properties of selective laser melted AlSi10Mg: Nano, micro, and macro properties," Proc. - 26th Annu. Int. Solid Free. Fabr. Symp. - An Addit. Manuf. Conf. SFF 2015, pp. 1026–1035, 2020.
- [43] K. Guan, Z. Wang, M. Gao, X. Li, X. Zeng, Effects of processing parameters on tensile properties of selective laser melted 304 stainless steel, Mater. Des. 50 (2013) 581–586, https://doi.org/10.1016/j.matdes.2013.03.056.
- [44] A. H. Maamoun, Y. F. Xue, M. A. Elbestawi, and S. C. Veldhuis, "Effect of selective laser melting process parameters on the quality of al alloy parts: Powder characterization, density, surface roughness, and dimensional accuracy," *Materials (Basel).*, vol. 11, no. 12, 2018, doi: 10.3390/ma11122343.
- [45] K.V. Yang, P. Rometsch, T. Jarvis, J. Rao, S. Cao, C. Davies, X. Wu, Porosity formation mechanisms and fatigue response in Al-Si-Mg alloys made by selective laser melting, Mater. Sci. Eng. A 712 (2018) 166–174, https://doi. org/10.1016/j.msea.2017.11.078.
- [46] D. Buchbinder, W. Meiners, N. Pirch, K. Wissenbach, J. Schrage, Investigation on reducing distortion by preheating during manufacture of aluminum components using selective laser melting, J. Laser Appl. 26 (1) (2014), https://doi.org/10.2351/1.4828755 012004.
- [47] A. Mauduit, S. Pillot, F. Frascati, Application study of AlSi10Mg alloy by selective laser melting: physical and mechanical properties, microstructure, heat treatments and manufacturing of aluminium metallic matrix composite (MMC), Metall. Res. Technol. 112 (6) (2015) 605, https://doi.org/10.1051/ metal/2015039
- [48] N. T. Aboulkhair, I. Maskery, C. Tuck, I. Ashcroft, and N. Everitt, "Nano-hardness and microstructure of selective laser melted AlSi10Mg scan tracks," Ind. Laser Appl. Symp. (ILAS 2015), vol. 9657, p. 965702, 2015, doi: 10.1117/ 12.2190015
- [49] I. Maskery, N.T. Aboulkhair, A.O. Aremu, C.J. Tuck, I.A. Ashcroft, R.D. Wildman, R.J.M. Hague, A mechanical property evaluation of graded density Al-Si10-Mg lattice structures manufactured by selective laser melting, Mater. Sci. Eng. A 670 (2016) 264–274, https://doi.org/10.1016/j.msea.2016.06.013.
- [50] M. Tang, P.C. Pistorius, Anisotropic mechanical behavior of AlSi10Mg parts produced by selective laser melting, Jom 69 (3) (2017) 516–522, https://doi. org/10.1007/s11837-016-2230-5.
- [51] B. Palumbo, F. Del Re, M. Martorelli, A. Lanzotti, and P. Corrado, "Tensile properties characterization of AlSi10Mg parts produced by direct metal laser sintering via nested effects modeling," *Materials (Basel)*, vol. 10, no. 2, 2017, doi: 10.3390/ma10020144.
- [52] B. Chen, S.K. Moon, X. Yao, G. Bi, J. Shen, J. Umeda, K. Kondoh, Strength and strain hardening of a selective laser melted AlSi10Mg alloy, Scr. Mater. 141 (2017) 45–49, https://doi.org/10.1016/j.scriptamat.2017.07.025.
- [53] R. Casati, M.H. Nasab, M. Coduri, V. Tirelli, M. Vedani, Effects of platform preheating and thermal-treatment strategies on properties of alsi10mg alloy processed by selective laser melting, Metals (Basel) 8 (11) (2018) 954, https:// doi.org/10.3390/met8110954.
- [54] M. Tang, P.C. Pistorius, Oxides, porosity and fatigue performance of AlSi10Mg parts produced by selective laser melting, Int. J. Fatigue 94 (2017) 192–201, https://doi.org/10.1016/j.ijfatigue.2016.06.002.

- [55] X. Ding, L. Wang, Heat transfer and fluid flow of molten pool during selective laser melting of AlSi10Mg powder: simulation and experiment, J. Manuf. Process. 26 (2017) 280–289, https://doi.org/10.1016/j.jmapro.2017.02.009.
- [56] C. Weingarten, D. Buchbinder, N. Pirch, W. Meiners, K. Wissenbach, R. Poprawe, Formation and reduction of hydrogen porosity during selective laser melting of AlSi10Mg, J. Mater. Process. Technol. 221 (2015) 112–120, https://doi.org/10.1016/j.jmatprotec.2015.02.013.
- [57] N.O. Larrosa, W. Wang, N. Read, M.H. Loretto, C. Evans, J. Carr, U. Tradowsky, M.M. Attallah, P.J. Withers, Linking microstructure and processing defects to mechanical properties of selectively laser melted AlSi10Mg alloy, Theor. Appl. Fract. Mech. 98 (2018) 123–133, https://doi.org/10.1016/j. tafmec.2018.09.011.
- [58] Y. Amani, S. Dancette, P. Delroisse, A. Simar, E. Maire, Compression behavior of lattice structures produced by selective laser melting: X-ray tomography based experimental and finite element approaches, Acta Mater. 159 (2018) 395–407, https://doi.org/10.1016/j.actamat.2018.08.030.
- [59] H. Asgari, A. Odeshi, K. Hosseinkhani, M. Mohammadi, On dynamic mechanical behavior of additively manufactured AlSi10Mg\_200C, Mater. Lett. 211 (2018) 187–190, https://doi.org/10.1016/j.matlet.2017.10.001.
- [60] C. Zhang, H. Zhu, Z. Hu, L. Zhang, X. Zeng, A comparative study on single-laser and multi-laser selective laser melting AlSi10Mg: defects, microstructure and mechanical properties, Mater. Sci. Eng. A 746 (January 2019) 416–423, https://doi.org/10.1016/j.msea.2019.01.024.
- [61] E. Cerri, E. Ghio, AlSi10Mg alloy produced by selective laser melting: relationships between vickers microhardness, rockwell hardness and mechanical properties, Metall. Ital. 112 (7–8) (2020) 5–17.
- [62] S. Beretta, M. Gargourimotlagh, S. Foletti, A. du Plessis, M. Riccio, Fatigue strength assessment of 'as built' AlSi10Mg manufactured by SLM with different build orientations, Int. J. Fatigue vol. 139 (February 2020), https:// doi.org/10.1016/j.ijfatigue.2020.105737 105737.
- [63] S. Parveen, R.U. Rao, D. K, and G. Telesang, "Investigation on Correlation between Microstructure and Mechanical Properties of Alsi10Mg Specimens by AM Technology," SSRN Electron. J., vol. 12, no. 10, pp. 325–329, 2021, doi: 10.2139/ssrn.3989415.
- [64] Y. Liu, C. Liu, W. Liu, Y. Ma, S. Tang, C. Liang, Q. Cai, C. Zhang, Optimization of parameters in laser powder deposition AlSi10Mg alloy using Taguchi method, Opt. Laser Technol. 111 (2019) 470–480, https://doi.org/10.1016/j. optlastec.2018.10.030.
- [65] Z. Dong, Y. Liu, W. Li, J. Liang, Orientation dependency for microstructure, geometric accuracy and mechanical properties of selective laser melting AlSi10Mg lattices, J. Alloys Compd. 791 (2019) 490–500, https://doi.org/ 10.1016/j.jallcom.2019.03.344.
- [66] N.T. Aboulkhair, N.M. Everitt, I. Ashcroft, C. Tuck, Reducing porosity in AlSi10Mg parts processed by selective laser melting, Addit. Manuf. 1 (2014) 77–86, https://doi.org/10.1016/j.addma.2014.08.001.
- [67] X. Liu, C. Zhao, X. Zhou, Z. Shen, W. Liu, Microstructure of selective laser melted AlSi10Mg alloy, Mater. Des. 168 (2019), https://doi.org/10.1016/ j.matdes.2019.107677 107677.
- [68] A. Salmi, E. Atzeni, L. Iuliano, M. Galati, Experimental analysis of residual stresses on AlSi10Mg parts produced by means of selective laser melting (SLM), Procedia CIRP 62 (2017) 458–463, https://doi.org/10.1016/j. procir.2016.06.030.
- [69] N. Read, W. Wang, K. Essa, M.M. Attallah, Selective laser melting of AlSi10Mg alloy: process optimisation and mechanical properties development, Mater. Des. 65 (2015) 417–424, https://doi.org/10.1016/j.matdes.2014.09.044.
- [70] L. Wang, X. Jiang, Y. Zhu, X. Zhu, J. Sun, B. Yan, An approach to predict the residual stress and distortion during the selective laser melting of AlSi10Mg parts, Int. J. Adv. Manuf. Technol. 97 (9–12) (2018) 3535–3546, https://doi. org/10.1007/s00170-018-2207-3.
- [71] A. Majeed et al., "An investigation into the influence of processing parameters on the surface quality of AlSi10Mg parts by SLM process," Proc. 2019 16th Int. Bhurban Conf. Appl. Sci. Technol. IBCAST 2019, pp. 143–147, 2019, doi: 10.1109/ IBCAST.2019.8667175.
- [72] J. Bao et al., "Defect evolution during high temperature tension-tension fatigue of SLM AlSi10Mg alloy by synchrotron tomography," *Mater. Sci. Eng. A*, vol. 792. p. 139809, 2020. doi: 10.1016/j.msea.2020.139809.
- vol. 792, p. 139809, 2020, doi: 10.1016/j.msea.2020.139809.

  [73] Y. Bai, Y. Yang, Z. Xiao, M. Zhang, D. Wang, Process optimization and mechanical property evolution of AlSiMg0.75 by selective laser melting, Mater. Des. 140 (2018) 257–266, https://doi.org/10.1016/j.matdes.2017.11.045.
- [74] A. Majeed, A. Ahmed, A. Salam, M.Z. Sheikh, Surface quality improvement by parameters analysis, optimization and heat treatment of AlSi10Mg parts manufactured by SLM additive manufacturing, Int. J. Light. Mater. Manuf. 2 (4) (2019) 288–295, https://doi.org/10.1016/j.ijlmm.2019.08.001.
- [75] A. Bin Anwar, Q.C. Pham, Selective laser melting of AlSi10Mg: Effects of scan direction, part placement and inert gas flow velocity on tensile strength, J. Mater. Process. Technol. 240 (2017) 388–396, https://doi.org/10.1016/j.jmatprotec.2016.10.015.
- [76] Y.J. Liu, Z. Liu, Y. Jiang, G.W. Wang, Y. Yang, L.C. Zhang, Gradient in microstructure and mechanical property of selective laser melted AlSi10Mg, J. Alloys Compd. 735 (2018) 1414–1421, https://doi.org/10.1016/ j.jallcom.2017.11.020.
- [77] A.A. Raus, M.S. Wahab, M. Ibrahim, K. Kamarudin, A. Ahmed, S. Shamsudin, Mechanical and physical properties of AlSi10Mg processed through selective laser melting, AIP Conf. Proc. 1831 (2017), https://doi.org/10.1063/ 1.4981168.

R.E. Gite and V.D. Wakchaure

Materials Today: Proceedings xxx (xxxx) xxx

- [78] P. Wei, Z. Wei, Z. Chen, J. Du, Y. He, J. Li, Y. Zhou, The AlSi10Mg samples produced by selective laser melting: single track, densification, microstructure and mechanical behavior, Appl. Surf. Sci. 408 (2017) 38–50, https://doi.org/10.1016/j.apsusc.2017.02.215.
- [79] M. Liu, N. Takata, A. Suzuki, M. Kobashi, Microstructural characterization of cellular AlSi10Mg alloy fabricated by selective laser melting, Mater. Des. 157 (2018) 478–491, https://doi.org/10.1016/j.matdes.2018.08.005.
- [80] N. Takata, H. Kodaira, A. Suzuki, M. Kobashi, Size dependence of microstructure of AlSi10Mg alloy fabricated by selective laser melting, Mater. Charact. 143 (October 2018) 18–26, https://doi.org/10.1016/ i.matchar.2017.11.052.
- [81] K.G. Prashanth, S. Scudino, T. Maity, J. Das, J. Eckert, Is the energy density a reliable parameter for materials synthesis by selective laser melting?, Mater Res. Lett. 5 (6) (2017) 386–390, https://doi.org/10.1080/ 21663831.2017.1299808.
- [82] L.P. Lam, D.Q. Zhang, Z.H. Liu, C.K. Chua, Phase analysis and microstructure characterisation of AlSi10Mg parts produced by Selective Laser Melting, Virtual Phys. Prototyp. 10 (4) (2015) 207–215, https://doi.org/10.1080/ 17452759.2015.1110868.
- [83] Z.H. Xiong, S.L. Liu, S.F. Li, Y. Shi, Y.F. Yang, R.D.K. Misra, Role of melt pool boundary condition in determining the mechanical properties of selective laser melting AlSi10Mg alloy, Mater. Sci. Eng. A 740–741 (2019) 148–156, https://doi.org/10.1016/j.msea.2018.10.083.
- [84] K. Kumar, S. Kumar, and M. Engineering, "Studies on hardness and tensile testing of AlSi10Mg produced by Selective Laser Melting 1," vol. 11, no. 6, 2020
- [85] K.G. Prashanth, J. Eckert, Formation of metastable cellular microstructures in selective laser melted alloys, J. Alloys Compd. 707 (2017) 27–34, https://doi. org/10.1016/j.jallcom.2016.12.209.
- [86] I. Rosenthal, A. Stern, N. Frage, Microstructure and mechanical properties of AlSi10Mg parts produced by the laser beam additive manufacturing (AM) technology, Metallogr. Microstruct. Anal. 3 (6) (2014) 448–453, https://doi. org/10.1007/s13632-014-0168-y.
- [87] H. Asgari, C. Baxter, K. Hosseinkhani, M. Mohammadi, On microstructure and mechanical properties of additively manufactured AlSi10Mg\_200C using recycled powder, Mater. Sci. Eng. A 707 (July 2017) 148–158, https://doi.org/ 10.1016/j.msea.2017.09.041.
- [88] N. Takata, H. Kodaira, K. Sekizawa, A. Suzuki, M. Kobashi, Change in microstructure of selectively laser melted AlSi10Mg alloy with heat treatments, Mater. Sci. Eng. A 704 (May 2017) 218–228, https://doi.org/ 10.1016/j.msea.2017.08.029.
- [89] E. Ghio and E. Cerri, "Work hardening of heat-treated alsi10mg alloy manufactured by single and double laser selective laser melting: Effects of layer thickness and hatch spacing," *Materials (Basel).*, vol. 14, no. 17, 2021, doi: 10.3390/ma14174901.
- [90] X. Yu, L. Wang, T6 heat-treated AlSi10Mg alloys additive-manufactured by selective laser melting, Procedia Manuf. 15 (2018) 1701–1707, https://doi. org/10.1016/j.promfg.2018.07.265.
- [91] P. Yang, M.A. Rodriguez, L.A. Deibler, B.H. Jared, J. Griego, A. Kilgo, A. Allen, D. K. Stefan, Effect of thermal annealing on microstructure evolution and mechanical behavior of an additive manufactured AlSi10Mg part, J. Mater. Res. 33 (12) (2018) 1701–1712, https://doi.org/10.1557/jmr.2018.82.
  [92] N.T. Aboulkhair, I. Maskery, C. Tuck, I. Ashcroft, N.M. Everitt, The
- [92] N.T. Aboulkhair, I. Maskery, C. Tuck, I. Ashcroft, N.M. Everitt, The microstructure and mechanical properties of selectively laser melted AlSi10Mg: the effect of a conventional T6-like heat treatment, Mater. Sci. Eng. A 667 (2016) 139–146, https://doi.org/10.1016/j.msea.2016.04.092.
- [93] U. Tradowsky, J. White, R.M. Ward, N. Read, W. Reimers, M.M. Attallah, Selective laser melting of AlSi10Mg: Influence of post-processing on the microstructural and tensile properties development, Mater. Des. 105 (2016) 212–222. https://doi.org/10.1016/j.matdes.2016.05.066.
- [94] L. Girelli, M. Tocci, M. Gelfi, A. Pola, Study of heat treatment parameters for additively manufactured AlSi10Mg in comparison with corresponding cast alloy, Mater. Sci. Eng. A 739 (2019) 317–328, https://doi.org/10.1016/j. msea 2018 10 026
- [95] A.H. Maamoun, M. Elbestawi, G.K. Dosbaeva, S.C. Veldhuis, Thermal post-processing of AlSi10Mg parts produced by Selective Laser Melting using recycled powder, Addit. Manuf. 21 (January 2018) 234–247, https://doi.org/10.1016/j.addma.2018.03.014.
- [96] F. Lv, L. Shen, H. Liang, D. Xie, C. Wang, Z. Tian, Mechanical properties of AlSi10Mg alloy fabricated by laser melting deposition and improvements via heat treatment, Optik (Stuttg) 179 (2019) 8–18, https://doi.org/10.1016/j. iileo.2018.10.112.
- [97] F. Sajadi, J.M. Tiemann, N. Bandari, A.C. Darabi, J. Mola, S. Schmauder, Fatigue improvement of alsi10mg fabricated by laser-based powder bed fusion through heat treatment, Metals (Basel) 11 (5) (2021) 1–17, https://doi.org/ 10.3390/met11050683.
- [98] A. Mertens, O. Dedry, M. M. Science, and R. B. St-jean, "Thermal treatments of AlSi10Mg processed by laser beam melting," Proc. 26th Int. Solid Free. Fabr. Symp., pp. 1007–1016, 2015, [Online]. Available: http://sffsymposium.engr. utexas.edu/2015TOC.
- [99] C. Zhang, H. Zhu, Y. Qi, X. Zeng, The effect of annealing on microstructure and mechanical properties of selective laser melting AlSi10Mg, IOP Conf. Ser.: Mater. Sci. Eng. 538 (1) (2019) 012023, https://doi.org/10.1088/1757-899X/ 538/1/012023.
- [100] E.W. Hovig, A.S. Azar, M. Mhamdi, K. Sørby, Mechanical properties of AlSi10Mg processed by laser powder bed fusion at elevated temperature,

- Miner. Met. Mater. Ser. 2 (2020) 395–404, https://doi.org/10.1007/978-3-030-36296-6-37
- [101] P. Qi, B. Li, T. Wang, L. Zhou, Z. Nie, Effect of heat treatment on microstructure and mechanical properties of alsi10mg alloy fabricated by selective laser melting, Mater. Sci. Forum vol. 1035 MSF (2021) 312–317, https://doi.org/ 10.4028/www.scientific.net/MSF.1035.312.
- [102] X. Jiang, W. Xiong, L. Wang, M. Guo, Z. Ding, Heat treatment effects on microstructure-residual stress for selective laser melting AlSi10Mg, Mater. Sci. Technol. (United Kingdom) 36 (2) (2020) 168-180, https://doi.org/ 10.1080/02670836.2019.1685770.
- [103] B.J. Mfusi, N.R. Mathe, P.A.I. Popoola, L.C. Tshabalala, Influence of stress relieving thermal cycles on AISI10Mg specimens produced by selective laser melting, IOP Conf. Ser.: Mater. Sci. Eng. 655 (1) (2019) 012027, https://doi. org/10.1088/1757-899X/655/1/012027.
- [104] L. Zhou, A. Mehta, E. Schulz, B. McWilliams, K. Cho, Y. Sohn, Microstructure, precipitates and hardness of selectively laser melted AlSi10Mg alloy before and after heat treatment, Mater. Charact. 143 (2018) 5–17, https://doi.org/10.1016/j.matchar.2018.04.022.
- [105] P. Van Cauwenbergh, A. Beckers, L. Thijs, B. Van Hooreweder, K. Vanmeensel, Heat treatment optimization via thermo-physical characterization of AlSi7Mg and AlSi10Mg manufactured by laser powder bed fusion (LPBF), Euro PM 2018 Congr. Exhib. (2018) 1–7.
- [106] N.E. Uzan, R. Shneck, O. Yeheskel, N. Frage, High-temperature mechanical properties of AlSi10Mg specimens fabricated by additive manufacturing using selective laser melting technologies (AM-SLM), Addit. Manuf. 24 (2018) 257–263, https://doi.org/10.1016/j.addma.2018.09.033.
- [107] A. Tridello, J. Fiocchi, C.A. Biffi, G. Chiandussi, M. Rossetto, A. Tuissi, D.S. Paolino, Influence of the annealing and defects on the VHCF behavior of an SLM AlSi10Mg alloy, Fatigue Fract. Eng. Mater. Struct. 42 (12) (2019) 2794–2807, https://doi.org/10.1111/ffe.13123.
- [108] T. Rautio, J. Mäkikangas, A. Mustakangas, K. Mäntyjärvi, Disk laser assisted surface heat treatments of AlSi10Mg parts produced by selective laser melting (SLM), Procedia Manuf. 36 (2019) 95–100, https://doi.org/10.1016/j. promfg.2019.08.014.
- [109] I. Rosenthal, R. Shneck, A. Stern, Heat treatment effect on the mechanical properties and fracture mechanism in AlSi10Mg fabricated by additive manufacturing selective laser melting process, Mater. Sci. Eng. A 729 (2018) 310–322, https://doi.org/10.1016/j.msea.2018.05.074.
- [110] T. Hirata, T. Kimura, T. Nakamoto, Effects of hot isostatic pressing and internal porosity on the performance of selective laser melted AlSi10Mg alloys, Mater. Sci. Eng. A vol. 772 (June 2020), https://doi.org/10.1016/j.msea.2019.138713 138713
- [111] N.T. Aboulkhair, I. Maskery, C. Tuck, I. Ashcroft, N.M. Everitt, On the formation of AlSi10Mg single tracks and layers in selective laser melting: Microstructure and nano-mechanical properties, J. Mater. Process. Technol. 230 (2016) 88–98, https://doi.org/10.1016/j.jmatprotec.2015.11.016.
- [112] J. Fiocchi, A. Tuissi, P. Bassani, C.A. Biffi, Low temperature annealing dedicated to AlSi10Mg selective laser melting products, J. Alloys Compd. 695 (2017) 3402–3409, https://doi.org/10.1016/j.jallcom.2016.12.019.
- [113] A. Iturrioz, E. Gil, M.M. Petite, F. Garciandia, A.M. Mancisidor, M. San Sebastian, Selective laser melting of AlSi10Mg alloy: influence of heat treatment condition on mechanical properties and microstructure, Weld. World 62 (4) (2018) 885–892, https://doi.org/10.1007/s40194-018-0592-8.
- [114] F. Alghamdi, M. Haghshenas, Microstructural and small-scale characterization of additive manufactured AlSi10Mg alloy, SN Appl. Sci. 1 (3) (2019), https://doi.org/10.1007/s42452-019-0270-5.
- [115] F. Trevisan *et al.*, "On the selective laser melting (SLM) of the AlSi10Mg alloy: Process, microstructure, and mechanical properties," *Materials (Basel).*, vol. 10, no. 1, 2017, doi: 10.3390/ma10010076.
- [116] K. Kempen, L. Thijs, J. Van Humbeeck, J.P. Kruth, Processing AlSi10Mg by selective laser melting: parameter optimisation and material characterisation, Mater. Sci. Technol. (United Kingdom) 31 (8) (2015) 917–923, https://doi.org/10.1179/1743284714Y.0000000702.
- [117] C.Y. Yap, C.K. Chua, Z.L. Dong, Z.H. Liu, D.Q. Zhang, L.E. Loh, S.L. Sing, Review of selective laser melting: materials and applications, Applied Physics Reviews 2 (4) (2015) 041101.
- [118] A. Boschetto, L. Bottini, F. Veniali, Roughness modeling of AlSi10Mg parts fabricated by selective laser melting, J. Mater. Process. Technol. 241 (2017) 154–163, https://doi.org/10.1016/j.jmatprotec.2016.11.013.
- [119] S.R. Ch, A. Raja, P. Nadig, R. Jayaganthan, N.J. Vasa, Influence of working environment and built orientation on the tensile properties of selective laser melted AlSi10Mg alloy, Mater. Sci. Eng. A 750 (January 2019) 141–151, https://doi.org/10.1016/j.msea.2019.01.103.
- [120] M. Tang, P.C. Pistorius, S. Narra, J.L. Beuth, Rapid solidification: selective laser melting of AlSi10Mg, Jom 68 (3) (2016) 960–966, https://doi.org/10.1007/ s11837-015-1763-3
- [121] C. Yan, L. Hao, A. Hussein, S.L. Bubb, P. Young, D. Raymont, Evaluation of light-weight AlSi10Mg periodic cellular lattice structures fabricated via direct metal laser sintering, J. Mater. Process. Technol. 214 (4) (2014) 856–864, https://doi.org/10.1016/j.jmatprotec.2013.12.004.
- [122] P. Wei, Z. Wei, Z. Chen, Y. He, J. Du, Thermal behavior in single track during selective laser melting of AlSi10Mg powder, Appl. Phys. A Mater. Sci. Process. 123 (9) (2017) 1–13, https://doi.org/10.1007/s00339-017-1194-9.
- [123] I. Rosenthal, A. Stern, N. Frage, Strain rate sensitivity and fracture mechanism of AlSi10Mg parts produced by Selective Laser Melting, Mater. Sci. Eng. A 682 (2017) 509–517, https://doi.org/10.1016/j.msea.2016.11.070.